Chapter 12
Prokaryotic Ferrous Iron Transport: Exploiting Pools of Reduced Iron Across Multiple Microbial Environments

Alex E. Sestok, Mark A. Lee, and Aaron T. Smith

Abstract Iron is essential to nearly all forms of life, but the redox activity of this element necessitates its cellular regulation. All iron-utilizing organisms require this nutrient to be tightly managed, which is accomplished by a suite of proteins and nucleic acids involved in the acquisition, the delivery, the storage, the regulation, and the export of this essential element. For infectious organisms, iron acquisition systems are commonly associated with intracellular growth, survival, and virulence of pathogens, which are dynamically able to modify their iron uptake strategies in response to changing host environments. The past few decades have been marked with an increased understanding of pathogenic ferric iron (Fe^{3+}) and heme acquisition. In contrast, though the necessity of ferrous iron (Fe^{2+}) transport for pathogenesis has been established, the precise details of this process remain enigmatic, and Fe^{2+} transporters remain unexploited as drug targets to combat drug-resistant organisms. This chapter will overview a current understanding of Fe^{2+} transport in microbes and highlight gaps in our knowledge that must be closed in order to establish a comprehensive understanding of unicellular Fe^{2+} metabolism.

12.1 Introduction

Throughout evolution, iron has emerged to become one of the most vital elements to virtually every living organism. In the modern era, biological systems that accomplish a suite of cellular processes, from aerobic cellular respiration, N_2 fixation, gene regulation, to even DNA biosynthesis make use of iron in all of its different forms (Sestok et al. 2018; Andrews et al. 2003; Lau et al. 2016). Iron has a diverse functionality and may be utilized as an ionic cofactor and bound by biological macromolecules, complexed within iron-sulfur clusters, or even chelated by organic molecules such as protoporphyrin-IX (heme) (Andrews et al. 2003; Sestok et al.

A. E. Sestok · M. A. Lee · A. T. Smith (✉)
Department of Chemistry and Biochemistry, University of Maryland, Baltimore County, Baltimore, MD, USA
e-mail: smitha@umbc.edu

C. J. Hurst (ed.), *Microbial Metabolism of Metals and Metalloids*, Advances in Environmental Microbiology 10, https://doi.org/10.1007/978-3-030-97185-4_12

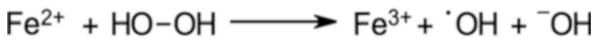

Fig. 12.1 The Fenton reaction. In the presence of hydrogen peroxide, ferrous iron (Fe^{2+}) is readily oxidized into ferric iron (Fe^{3+}), forming both a hydroxyl radical and a hydroxide ion in the process. Hydroxyl radicals can lead to harmful and deleterious oxidation of biomolecules if uncontrolled

2018). Biology is replete with essential proteins and enzymes that use some or even all forms of this element. For example, iron-dependent ribonucleotide reductases reduce ribonucleotides to deoxyribonucleotides by making use of a diiron center that shuttles electrons for nucleotide reduction (Torrents 2014). Nitrogenase enzymes, which allow bacteria to fix N_2, utilize multiple iron-sulfur clusters ([4Fe-4S], [8Fe-7S], and [7Fe-Mo-9S]) throughout the fixation cycle (Hu and Ribbe 2015). Hemoglobin (Wittenberg et al. 2002) and myoglobin (Brunori 2010) both require a heme *b* cofactor for O_2 transport. This large assortment of iron-containing proteins clearly demonstrates the dependence on iron for the survival of organisms found across every kingdom life.

Iron is capable of fulfilling such a dynamic role in life because of its abundance on earth and its versatility as an element, if it can be acquired. For example, iron is the most abundant transition metal on earth's crust, comprising up to ca. 5% of the outermost layer of the planet. However, unlike oxygen, silicon, and aluminum, which make up significantly more of the outer layer of Earth, the chemistry of iron is much more diverse. Iron can sample multiple oxidation and spin states, and its electronic reactivity can be modulated by the ligands responsible for binding the metal in biological macromolecules. This tunability controls the redox potential of iron, which can span from ca. −300 mV to +700 mV (i.e., a 1 V range), affording organisms the potent oxidizing and reducing iron-based cofactors necessary to accomplish a wide swath of complex chemical transformations (Andrews et al. 2003). However, despite its abundance, acquisition of this essential element is no small feat. While Fe^{3+} (ferric iron) predominates in oxic environments, it is highly insoluble (ca. 10^{-18} M at pH 7.0) and easily forms recalcitrant ferric oxides and hydroxides, whereas Fe^{2+} (ferrous iron) is more soluble (as high as 0.1 M at pH 7.0) but is present under anoxic and reducing conditions and is susceptible to rapid oxidation (Fig. 12.1) (Andrews et al. 2003; Krewulak and Vogel 2008; Winterbourn 1995), presenting a conundrum to many organisms. Given the critical importance of iron to life, decades of research have focused on the mechanisms of iron transport, utilization, and even regulation. Much of this research has centered around bacterial iron homeostasis due to its simpler mode of study and spurred by the strong relationship between iron availability and bacterial pathogenesis.

In order to utilize iron, this nutrient must first be obtained from the environment and subsequently transported to the necessary locations within the cell where the metal is needed. This process requires organisms to employ diverse iron sequestration systems capable of functioning under a variety of different physiological niches and in different environments to exploit whatever pools of iron may be available (Andrews et al. 2003; Sestok et al. 2018). In Gram-negative bacteria, Fe^{3+} can be scavenged by siderophores, low molecular weight molecules with a high affinity for

Fe^{3+} ($K_{aff} > 10^{30}$ M^{-1}) that are secreted into the extracellular space. Siderophores compete for Fe^{3+} already bound to host proteins and help to keep Fe^{3+} soluble during the transport process. Uptake of the Fe^{3+}-siderophore complex from the extracellular space into the periplasm typically occurs via a TonB-dependent outer membrane receptor coupled to the proton motive force (PMF) and often specific to the siderophore (Andrews et al. 2003; Sestok et al. 2018; Krewulak and Vogel 2008; Chu et al. 2010; Ellermann and Arthur 2017). Periplasmic binding proteins then chaperone the complex to a dedicated inner membrane protein, typically an ATP-binding cassette (ABC) transporter. Once in the cytoplasm, Fe^{3+} can be reduced to Fe^{2+} or the siderophore can be degraded to release the iron (Cain and Smith 2021). Uptake of siderophores is similar in Gram-positive bacteria, except that the Fe^{3+}-siderophore complex binds to a membrane anchored lipoprotein before being handed off to the ABC transporter (Andrews et al. 2003; Sestok et al. 2018; Krewulak and Vogel 2008; Chu et al. 2010; Ellermann and Arthur 2017). Heme sequestered from host proteins also serves as a form of iron to bacteria; however, because of its dramatically different composition from that of free iron, dedicated heme acquisition and transport systems are necessary. Pathogenic bacteria can employ hemolysins and proteases to release heme from red blood cells. Bacteria can then bind heme by using dedicated hemophores or by utilizing outer membrane receptors to transport host heme-binding proteins into the cell (Andrews et al. 2003; Sestok et al. 2018; Krewulak and Vogel 2008; Huang and Wilks 2017; Richard et al. 2019). The heme-hemophore complex is transported across the outer membrane in a TonB-dependent manner, similar to siderophore uptake. ABC transporters may also shuttle hemophores across the cytoplasmic membrane where the heme is degraded by heme oxygenase (HO), releasing iron and protoporphyrin catabolites (Andrews et al. 2003; Sestok et al. 2018; Krewulak and Vogel 2008; Huang and Wilks 2017; Richard et al. 2019). Both ferric iron and heme serve as indispensable iron sources for bacteria and have been well studied.

Recently, it has become apparent that Fe^{2+} acquisition and utilization are both necessary for bacterial growth, survival, and in some cases, for pathogenesis (Sestok et al. 2018; Andrews et al. 2003). However, bacterial ferrous iron uptake is not as well characterized as that of ferric iron and heme uptake. Ferrous iron is likely to be the dominant iron source for bacteria that thrive in microaerophilic or anoxic environments, such as those living within biofilms, and those living in acidified, reducing environments like the stomach. Additionally, there is evidence that Fe^{3+} utilization is linked to Fe^{2+} transport, especially in cases where organisms utilize non-native siderophores known as xenosiderophores (Cain and Smith 2021; Schröder et al. 2003). These molecules can be transported across the outer membrane through TonB-dependent receptors specific for the xenosiderophores or through outer membrane receptors with broad specificity for several siderophores (Cornelis 2010; Sheldon and Heinrichs 2015). However, since organisms that can utilize xenosiderophores often lack siderophore-specific, inner membrane transporters, they must therefore either reduce Fe^{3+} to Fe^{2+}, through the use of a ferric iron reductase (Cain and Smith 2021), or degrade the xenosiderophore within the periplasm. In either scenario, transport of Fe^{2+} into the cytoplasm requires dedicated

and selective Fe^{2+} transporters. Ferric iron reductases can also function extracellularly and exhibit broad substrate specificity for different Fe^{3+}-chelates, necessitating Fe^{2+} transport across the outer membrane. The process of Fe^{3+} reduction may involve a flavin cofactor (soluble ferric reductases) or heme *b* (membrane ferric reductases) to transport electrons for iron reduction (Cain and Smith 2021). Thus ferric iron reductases allow for organisms to generate and to utilize Fe^{2+} even in oxic environments (Schröder et al. 2003). Ferrous iron transporters have been discovered in many kingdoms of life, but most remain under- or poorly-studied. This chapter focuses on how microbes specifically exploit the presence of pools of reduced, ferrous iron in the environment to fulfill metabolic needs and to establish infection within host niches. Importantly, while reduced iron availability has changed throughout Earth's evolution, microbes have adapted and maintained the ability to acquire this necessary nutrient through conserved mechanisms across multiple microbial environments.

12.2 Iron and Bacteria on Early Earth

Bacteria first appeared on Earth approximately 4 billion years ago and thrived in an environment remarkably different from that of today's (DeLong and Pace 2001). The presence of *b*anded *i*ron *f*ormations (BIFs) have shown that Earth's first oceans were ferruginous (rich in iron), and these mineral "snapshots" offer insight into how the composition of Earth's oceans have changed throughout Earth's evolution (Li et al. 2018; Schad et al. 2019; Konhauser et al. 2017). While there are multiple mechanisms by which iron oxidation to promote BIFs could have transpired, one prevailing hypothesis suggests formation occurred through oxidation of iron by bacteria, such as *Gallionella ferruginea*, as fossilized bacteria have been discovered co-deposited within BIFs (Konhauser et al. 2017). These ancient bacteria were micro-aerophilic, being either (or both) nitrate-reducing, phototrophic ferrous iron (Fe^{2+})-oxidizers or ferric iron (Fe^{3+})-reducers (Schad et al. 2019). Studies have shown that bacteria inhabiting the surface of the early oceans likely utilized Fe^{2+} oxidation to produce Fe^{3+}-containing minerals as protective mechanisms against harmful UV-radiation prior to the more modern development of the ozone layer (Gauger et al. 2015, 2016). Fe^{2+} was also proposed to be involved in the photosynthetic process known as photoferrotrophy, whereby UV-radiation facilitated oxidation of dissolved Fe^{2+} species that was subsequently coupled to several essential assimilatory processes, such as reduced carbon fixation, CO_2 fixation, and even N_2 fixation (Konhauser et al. 2017; Schad et al. 2019). However, changes in Earth's atmospheric composition quickly altered metal speciation on the surface and within the oceans.

The presence of significant levels of atmospheric O_2 during the *G*reat *O*xygenation *E*vent (GOE) was thought to have appeared around 2.4 billion years ago, though this estimation is complicated by the lack of consensus as to exactly when and where cyanobacterial photosynthesis began (either in the early Archean Eon or

the late Paleoproterozoic Eon) (Schad et al. 2019; Glass 2015; Shih 2019). Regardless of the precise date, the emergence of photosynthetic cyanobacteria resulted in the release of substantive amounts of O_2 into the atmosphere and dissolved within the oceans. This increase in O_2 caused dramatic changes in early microbial environments, leading to pressures on anaerobic metabolizers and the alteration of metal bioavailability, chiefly due to O_2's effects on oxidation state speciation of multiple essential transition metals.

Notably and especially affected was iron, as the GOE heavily altered the iron biogeochemical cycle (Glass 2015; Schad et al. 2019; Shih 2019). As the distribution of iron shifted from the soluble Fe^{2+} form to the insoluble Fe^{3+} form, microbes were pressured to adapt to fulfill their metabolic needs or perish. As fossil records do not indicate a mass bacterial extinction event, it is clear that microbes overcame this challenge through evolved mechanisms of metal scavenging, metal storage, metal substitution, and a metabolic shift towards different metal speciation (Glass 2015). However, not every planetary niche was transformed by the GOE. Studies suggest that some ferruginous environments were preserved, and microbes in those environments likely maintained a necessity for Fe^{2+}, which was still present in relatively high concentrations in these locations (Derry 2015; Konhauser et al. 2017).

Despite its difficulty to obtain from the environment, iron still serves as an indispensable metal cofactor for many enzymes (Glass 2015); however, before iron may be incorporated into proteins and enzymes and used in cofactor biosynthesis, iron must first be solubilized and transported into the cell. As microbes may encounter multiple forms of environmental iron, it is unsurprising that this process is accomplished by a variety of iron acquisition systems. A large number of microbial iron uptake mechanisms have been discovered and characterized extensively. Consistent with the essential nature of iron as a micronutrient, these acquisition systems have been determined to be essential for microbial growth, survival, and even virulence. However, most studies have focused on mechanisms of Fe^{3+} acquisition, such as Fe^{3+}-siderophore transport, heme transport, and even the acquisition of host Fe^{3+}-binding proteins from the extracellular space. In stark contrast, much less is known about Fe^{2+} uptake despite the importance of Fe^{2+} for the survival of both the first organisms that inhabited the planet and numerous bacteria located in modern-day ferruginous environments.

12.3 Fe^{2+} Acquisition Systems

Several Fe^{2+} uptake systems have been identified in bacteria, and it is likely that more exist that have not yet been characterized (Fig. 12.2). Furthermore, while some transport systems are specific to Fe^{2+} transport (such as the Feo and Efe systems), other systems mediate the transport of multiple divalent metal ions such as Mn^{2+}, Cu^{2+}, Zn^{2+}, Ni^{2+}, and Co^{2+}. Given the different coordination properties of Fe^{2+} and Fe^{3+}, and the different environments in which these two ions are obtained, different machinery is required for the transport of Fe^{2+} and Fe^{3+}. For instance, siderophores

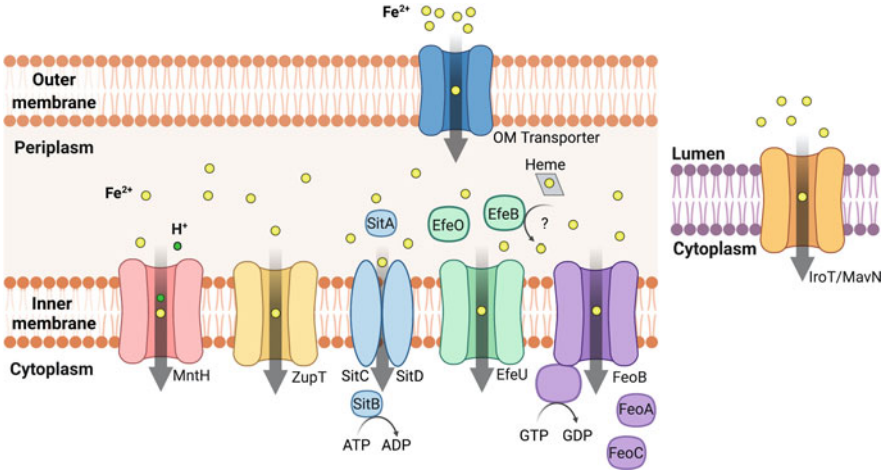

Fig. 12.2 A cartoon of the currently known bacterial ferrous iron uptake systems, depicted here for a Gram-negative bacterium. Fe^{2+} is transported into the periplasm via an unidentified outer membrane transporter where it is then taken up by one or multiple inner membrane Fe^{2+} transport systems. MntH, ZupT, and SitABCD transport multiple divalent metal ions in addition to H^+, while EfeUOB is specific for Fe^{2+}, but is only functional in pathogenic bacteria. IroT/MavN has been identified in *Legionella* species and functions at the LCV membrane. In contrast, Feo is the most widespread, dedicated Fe^{2+} transport system in bacteria. Figure created with BioRender

typically coordinate Fe^{3+} in an octahedral geometry with hexadentate ligands and are highly specific for hard Lewis acids (Andrews et al. 2003; Krewulak and Vogel 2008). Such a molecule does not coordinate the softer Lewis acid Fe^{2+} with the same affinity or even the same geometry in many cases. Additionally, because Fe^{2+} is much more soluble than Fe^{3+}, it is unnecessary for the ion to be bound to large chelates during the transport process but may instead be transported as an ion via Fe^{2+}-specific transporters. Though not an exhaustive list, some of the best characterized Fe^{2+} transporters are described below.

12.3.1 Natural Resistance-Associated Macrophage Proteins (NRAMPs) and Divalent Metal Transporters (DMTs)

*N*atural *r*esistance-*a*ssociated *m*acrophage *p*roteins (NRAMPs) are a family of *d*ivalent *m*etal *t*ransporters (DMTs), also known as *sol*ute *c*arriers (SLCs), involved in both eukaryotic and prokaryotic iron homeostasis. Eukaryotes express two separate NRAMPs, NRAMP1 (or SLC11A1) and NRAMP2 (or SLC11A2/DMT1). NRAMP1 is phagosomally-expressed and aids in the fight against pathogens by sequestering iron (among other transition metals) from the invading bacterium during phagocytosis by macrophages, whereas NRAMP2 facilitates the absorption of dietary iron and is critical in maintaining iron homeostasis (Ehrnstorfer et al.

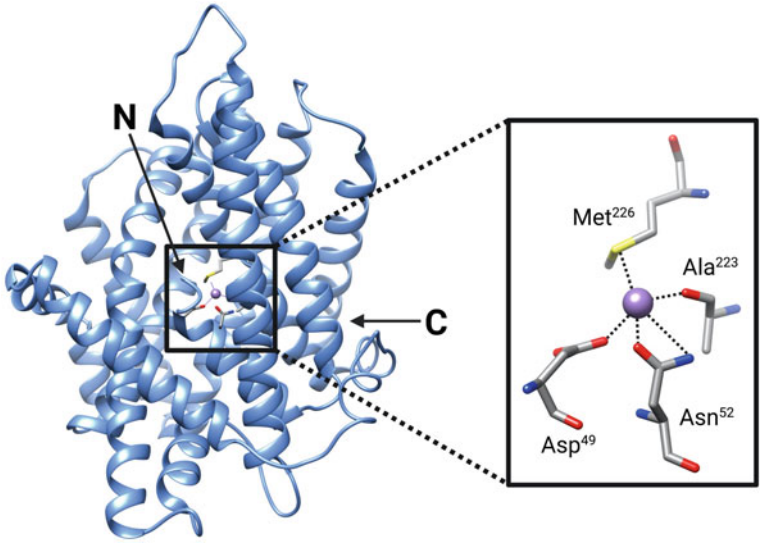

Fig. 12.3 X-ray crystal structure of *Sca*DMT bound to Mn^{2+} (PDB ID: 4WGW). Mn^{2+} (purple sphere) is coordinated by side chains from Met, Asp, and Asn residues, and a peptidyl oxygen from Ala (expanded region). 'N' and 'C' represent the N- and C-termini respectively. Figure created with BioRender

2014; Bozzi et al. 2016). Bacterial NRAMP homologues constitute three "clades" (A, B, C) and display a high degree of sequence conservation to their eukaryotic counterparts, suggesting that their metal specificity and transport mechanisms may be similar to those exhibited in eukaryotes (Ehrnstorfer et al. 2014; Bozzi et al. 2016).

Recent studies have sought to understand the mechanism of NRAMP-mediated divalent metal ion transport through a combination of structural and biochemical techniques. In an X-ray crystal structure of a truncated *Staphylococcus capitis* DMT (*Sca*DMT) (belonging to clade C but lacking 41 N-terminal residues) the *t*rans*m*embrane (TM) I region contains an inverted repeat of the first five TM helices (known as a LeuT fold) and an unstructured region in the first helix in the inverted repeat (between helix 1 and helix 6), providing the coordinating ligands for metal substrates (Ehrnstorfer et al. 2014). The metal-coordinating residues of a metal-bound state were initially determined by solving the X-ray crystal structure of Mn^{2+}-bound *Sca*DMT (PDB ID: 4WGW), which revealed the side chains of Met, Asp, and Asn (conserved residues in human DMT1) as well as the peptidyl carbonyl oxygen all bound to Mn^{2+} (Fig. 12.3) (Ehrnstorfer et al. 2014). Further structural and functional characterization of *Sca*DMT demonstrated binding of Fe^{2+}, Co^{2+}, Ni^{2+}, Cd^{2+}, Pb^{2+}, and Cu^{2+} (albeit in a slightly shifted position). Mn^{2+}, Co^{2+}, Ni^{2+}, and Cd^{2+} could be transported into *Sca*DMT-containing liposomes, although Fe^{2+} transport was not confirmed in this study (Ehrnstorfer et al. 2014). Intriguing follow-up studies demonstrated that the coordinating Met lends itself importantly to specificity by

discriminating against alkali earth metals (Bozzi et al. 2016), which could be a common theme amongst Fe^{2+} transporters.

An X-ray crystal structure of *Deinococcus radiodurans* NRAMP (*Dra*NRAMP), a member of prokaryotic clade A NRAMPS, similarly displayed a LeuT fold in an inward-facing conformation but included the missing N-terminal residues from the *Sca*DMT structure. The position of TM helix 1a to that of 1b is striking as the angle between the two helices is 103°. This bent conformation is believed to create an "aqueous vestibule" that may allow for a water molecule to coordinate metal bound between helices 1 and 6 (Bozzi et al. 2016). Furthermore, molecular snapshots obtained from cysteine accessibility scanning suggest that *Dra*NRAMP undergoes a series of conformational changes to facilitate the transport of divalent metal ions through an extracellular metal-permeation pathway before reaching the metal-binding site, which could be a common mechanism among NRAMPs (Bozzi et al. 2016). While more structural information will be necessary to elucidate the full mechanism of divalent metal transport in these proteins and to characterize mutations resulting in disease states, the current structures and functional analyses have contributed to understanding how a broad range of metal substrates can be recognized, demonstrating the high flexibility and substrate promiscuity of some transporters. These models could prove useful for other uncharacterized transporters.

The H^+-dependent *man*ganese *t*ransport system (MntH) (Fig. 12.2, pink) is a NRAMP homolog first identified in *E. coli* in 1969 (Silver and Kralovic 1969; Silver et al. 1970; Bhattacharyya 1970; Makui et al. 2000). Though MntH has a preference for Mn^{2+}, it has also been linked to the transport of Fe^{2+}, and cells overexpressing MntH accumulate Fe^{2+} via active transport, as observed by in vivo $^{55}Fe^{2+}$ uptake experiments. In this study, $^{55}Fe^{2+}$ uptake could also be inhibited by Mn^{2+} and Zn^{2+} when supplied at a 100-fold molar excess or by the addition of protonophores (Makui et al. 2000). Similar experiments performed to monitor in vivo $^{54}Mn^{2+}$ uptake reveal the same proton-dependent uptake as $^{55}Fe^{2+}$. However, $^{54}Mn^{2+}$ accumulated to approximately ten-fold higher concentration over $^{55}Fe^{2+}$, demonstrating MntH's specificity for Mn^{2+} (Makui et al. 2000). In addition, the overexpression of MntH allowed cells to accumulate Cd^{2+}, Zn^{2+}, and Co^{2+} as well as Ni^{2+} and Cu^{2+}, but to a lesser extent, suggesting that Ni^{2+} and Cu^{2+} represent poor MntH substrates (Makui et al. 2000).

Another study measured the apparent K_M of Mn^{2+} uptake to be 1 μM in *E. coli* and 100 nM in *Salmonella typhimurium*. In *S. typhimurium*, transport of Mn^{2+} was not inhibited by Na^+, K^+, Mg^{2+}, or Ca^{2+}. Contrary to the results described above, Ni^{2+}, Cu^{2+}, and Zn^{2+} required a 1000-fold excess to inhibit Mn^{2+} uptake, suggesting they are not potential substrates of MntH. However, Cd^{2+} greatly inhibited Mn^{2+} transport (Kehres et al. 2000). Similar observations were seen for *Ec*MntH. Unsurprisingly, though Fe^{2+} could be accumulated by both *Ec*- and *St*MntH, transport of Fe^{2+} was significantly inhibited by Mn^{2+}. These results corroborate MntH's preference for Mn^{2+} even though it is capable of transporting other divalent metal ions (Kehres et al. 2000). Consistent with this specificity, regulation of *Ec*MntH is accomplished via the Mn^{2+}-responsive transcriptional regulator, MntR, which belongs to the DtxR family, although partial repression by Fe^{2+}-Fur was also

observed, indicating cross-talk between Mn and Fe homeostasis in this organism (Patzer and Hantke 2001).

The ZupT divalent metal transporter (Fig. 12.2, yellow) from *E. coli* is also believed to transport Fe^{2+} in addition to Zn^{2+} and other metals (Grass et al. 2002, 2005a). This protein belongs to the *z*inc-*r*egulated *t*ransporter (*Z*RT), *i*ron-*r*egulated *t*ransporter (*I*RT)-like *p*roteins known as the ZIP family. This family has been identified in animals, plants, protists, and fungi, and these transporters are known to mobilize Fe^{2+}, Zn^{2+}, Mn^{2+}, and Cd^{2+} (Guerinot 2000). ZupT is the first member of this family to be found in the bacterial kingdom (Guerinot 2000; Grass et al. 2002, 2005a). Strains of *E. coli* defective for all other iron transport systems except for ZupT were able to grow in the absence of metals and in the presence of Mg^{2+}, Zn^{2+}, Mn^{2+}, and Fe^{3+}. ^{55}Fe uptake assays demonstrated that *E. coli* strains defective for iron transport but harboring an inducible plasmid for ZupT demonstrated the ability to import Fe^{2+} (Grass et al. 2005a). ZupT was also able to transport Co^{2+} in a strain carrying an additional deletion for CorA, a Co^{2+} transporter. Further demonstrating its substrate promiscuity, ZupT is also believed to transport Mn^{2+}, but at a much lower affinity (Grass et al. 2005a). When compared to MntH and Feo (vide infra), the ZupT protein was not as efficient for Fe^{2+} transport, suggesting that ZupT could be a secondary Fe^{2+} transporter in *E. coli* (Grass et al. 2005a). Despite evidence of broad divalent metal ion substrate specificity by ZupT, this protein remains largely uncharacterized, and more work is needed to understand the molecular details of the metal binding and transport process to determine how ZupT contributes to Fe^{2+} uptake in *E. coli*.

12.3.2 ATP-Binding Cassette (ABC) Transporters

The *Salmonella i*ron *t*ransporter (*sit*) operon in *Salmonella typhimurium* was first identified in 1999 in the centisome 63 pathogenicity island and has high homology to the *yfe* system (Bearden et al. 1998) from *Y. pestis*. The *sit* operon encodes for four proteins: SitA, a putative periplasmic binding protein with homology to YfeA; SitB, the ABC transporter; and SitC and SitD, putative integral membrane permeases with homology to YfeC and YfeD (Fig. 12.2, blue) (Zhou et al. 1999). To test the role of the Sit system in Fe^{2+} transport, *St*SitABCD was introduced into an enterobactin-deficient strain of *E. coli*. Expression of the *sit* operon rescued a growth defect of the *E. coli* strain in iron-limited media (Zhou et al. 1999). A Δ*sitBCD* deletion strain was tested in vivo to determine the effect of the Sit system on *S. typhimurium* virulence; however, no difference in the virulence of the Δ*sitBCD* deletion strain was detected, which is likely the result of redundant iron transport systems present in *S. typhimurium* (Zhou et al. 1999). A different study demonstrated that *sitABCD* is induced in mouse liver when infected intraperitoneally, but induction of *sitABCD* was much lower in other organs when mice were infected orally. These results suggest that *sitABCD* is expressed during late-stage infection, after invasion of the intestines (Janakiraman and Slauch 2000). In contrast to previous results,

S. typhimurium strains bearing a *sitA* mutation, which was polar on downstream *sit* genes, exhibited growth and survival defects in mice (Janakiraman and Slauch 2000). Additionally, the *sit* operon was found to be controlled by Fe^{2+} and Fur, though another study determined MntR and Mn^{2+} also regulated the *sit* operon (Zhou et al. 1999; Janakiraman and Slauch 2000; Ikeda et al. 2005). Similar regulation is also observed for the Yfe system of *Y. pestis* (Bearden et al. 1998; Perry et al. 2012).

Though the Sit system was first identified as an ATP-dependent Fe^{2+} uptake system, it is also able to transport Mn^{2+} with a higher affinity than that of Fe^{2+}. Similar to MntH, the apparent affinity of $^{54}Mn^{2+}$ transport by *S. typhimurium* SitABCD was 0.1 μM and was not affected by pH. In contrast to the association constant, maximal Mn^{2+} transport was pH-dependent and increased at alkaline pH (Kehres et al. 2002), and Fe^{2+} inhibition of Mn^{2+} transport was also observed. Somewhat similarly, transport of $^{55}Fe^{2+}$ by SitABCD occurred in a pH-dependent manner and was inhibited by Mn^{2+} though inhibition was not pH-dependent (Kehres et al. 2002). Cd^{2+}, Zn^{2+}, Co^{2+}, Cu^{2+}, Ni^{2+} and Fe^{3+} were also tested for their ability to inhibit Mn^{2+} transport with Cd^{2+} and Zn^{2+} being the most potent inhibitors (Kehres et al. 2002). Whether Fe^{2+} is a natural substrate of the Sit system remains debated and may be dependent upon the conditions under which the Sit system is expressed.

12.3.3 Oxidase-Dependent Fe^{2+} Transporters (OFeTs)

The *e*lemental *fe*rrous iron *u*ptake (EfeU) protein (also known as YcdN) is a unique Fe^{2+} transporter that has been well characterized but is operative only in select pathogenic species (Fig. 12.2, green). Belonging to the *ycdNOB* operon, EfeU is homologous to the yeast high-affinity ferric iron permease protein Ftr1p that belongs to the *o*xidase-dependent *i*ron *t*ransporters (OFeTs) (Grosse et al. 2006). These transporters are part of a larger family of proteins known as the *i*ron/*l*ead t*r*ansporter (ILT) superfamily that transports $Fe^{2+/3+}$ and Pb^{2+} (Saier et al. 2006, 2021). Yeast Ftr1p contains an REXXE iron-binding motif, similar to other metal transporters (Stearman et al. 1996; Severance et al. 2004; Grosse et al. 2006), and yeast Ftr1p functions in tandem with a multicopper ferroxidase, Fet3p, and an extracellular reductase, Fre, to transport iron. Fre must first reduce Fe^{3+} to Fe^{2+}, at which point Fet3p binds the metal and oxidizes the ion back to Fe^{3+}. A hand-off of the metal occurs between Fet3p and Ftr1p (Askwith et al. 1994; Askwith and Kaplan 1997). By comparison, in *E. coli*, the *efeUOB* operon (also termed the *ycdNOB* operon) is polycistronic and is expressed under iron-deplete conditions. Expression of *efeUOB* is controlled by FUR and is not regulated in response to O_2 (Grosse et al. 2006; Cao et al. 2007). When pH-dependent expression of *efeU* was determined, *efeU* displayed higher expression at lower pH (pH = 5.0), under which Fe^{2+} would be stabilized, than at higher pH (pH = 8.0) for both iron-deplete and iron-replete conditions. This pH-dependent regulation is accomplished by *cpxAR*, a

two-component sensor regulator, where CpxA is a histidine kinase localized to the inner membrane and CpxR is an OmpR-like response regulator (Cao et al. 2007). Given EfeU's homology to yeast Ftr1p, these results could provide insight into the mechanism of iron uptake by EfeU.

EfeU is a 276 amino acid protein predicted to have seven TM helices with a periplasmic N-terminal domain and a cytoplasmic C-terminal domain. REXXE iron binding motifs are located in TM helix 1 and TM helix 4. Additionally, an ≈40 amino acid periplasmic extension is one of two glutamate-rich periplasmic regions located between TM helix 6 and TM helix 7. The TM region is devoid of both negatively charged residues and His residues and, with the exception of the REXXE motifs and some Met residues, appears to be lacking in other metal-binding amino acids (Grosse et al. 2006). To test the important of the REXXE motifs in EfeU, each motif was individually mutated. Regardless of which motif harbored the mutation, an iron uptake deficient strain of *E. coli* was unable to grow. These results suggest that mutation of the REXXE motifs rendered the organism incapable of binding and transporting iron for growth under experimental conditions. EfeU is also believed to be highly-specific for iron, as EfeU was found to not be involved in the transport of Zn^{2+}, Pb^{2+}, or Cu^{2+}(Grosse et al. 2006), and a preference for Fe^{2+} over Fe^{3+} was also observed, indicating high specificity of EfeU (Cao et al. 2007). EfeU was also tested for in vitro metal transport into proteoliposomes to verify which oxidation state of iron is transported by the protein. Using Phen Green SK as a fluorescence reporter for metal transport into the proteoliposomes, only Fe^{2+} translocation was observed. This transport process is believed to occur via facilitated diffusion, though the energy coupling process has not been fully elucidated (Grosse et al. 2006). It is also possible that additional factors may contribute to Fe^{2+} binding and transport of EfeU, such as the proteins EfeB and EfeO.

EfeB is believed to be a periplasmic paralog of the dye-decolorizing peroxidases. In *E. coli*, the EfeB protein contains a twin-arginine signal sequence suggesting the protein is translocated across the cytoplasmic membrane to the periplasm via the *t*win-*a*rginine-*t*ranslocation (Tat) system. However, some EfeB has also been detected in the cytoplasm. EfeB is known to be a heme *b* containing-protein regardless of compartmental localization (Sturm et al. 2006). EfeB was confirmed to have peroxidase activity by monitoring H_2O_2-dependent oxidation of guaiacol, a naturally-occurring organic compound; however, no specific substrate of EfeB was identified (Sturm et al. 2006). A later study evaluated the ability of EfeB to degrade heme for iron utilization in *E. coli*. Soluble fractions of cell lysates containing overexpressed EfeB were able to extract iron from hemin (Létoffé et al. 2009). As no other protoporphyrin metabolites were identified upon iron release from heme by YfeX or EfeB, it was suggested that both proteins have deferrochelation activity and thus leave the protoporphyrin ring intact. It is possible that, in the context of the Efe system, EfeB serves to demetallate heme to provide iron, likely Fe^{2+}, to EfeU for transport into the cytoplasm (Létoffé et al. 2009). Both EfeB and its paralog YfeX were subsequently found to be essential for exogenous heme iron acquisition in vivo and strains lacking either *yfeX* or *efeB* or both could utilize exogenous heme when complemented with *pigA*, a heme oxygenase from *Pseudomonas aeruginosa*,

suggesting their functions are related to the release of iron from heme (Létoffé et al. 2009). In the absence of functional heme-uptake systems, overexpression of a functional *efeUOB* operon allowed for heme acquisition in *E. coli*.

To further investigate the function of EfeB, the protein was crystallized in complex with heme and the structure was determined to 1.95 Å resolution (PDB ID: 2Y4E). The asymmetric unit consisted of homodimeric EfeB (residues 48–422) in which both molecules were bound to heme (Liu et al. 2011). The crystal structure revealed that EfeB is structurally similar to the de-colorizing peroxidase enzymes and adopts a ferredoxin-like fold. The N-terminal and C-terminal domains of EfeB are connected via a 22-amino acid loop termed the switch loop. This loop helps to stabilize the heme-EfeB interaction solely by interaction with the heme cofactor, potentially to mediate demetallation of the heme cofactor (Liu et al. 2011). While EfeB removes iron from heme in vivo, resulting in the accumulation of protoporphyrin-IX, purified EfeB does not display this enzymatic activity, likely due to the absence of an additional cofactor or cosubstrate. Though EfeB is undeniably involved in the iron transport process, the mechanism of demetallation, and what additional factors may be involved in this process (such as peroxidase activity), remain unknown. Given the role of iron in bacterial pathogenesis, EfeB could serve as an antibacterial target, an endeavor that would be facilitated by further characterization of EfeB and its homologs.

EfeO (YcdO) is a predicted periplasmic protein that has also been found to be similar to dye-decolorizing peroxidases. Similar to EfeB, *E. coli* EfeO was also predicted to be a Tat-substrate; however, its twin-arginine signal sequence is not conserved amongst other EfeO homologs (Sturm et al. 2006). Though EfeO is not well characterized, EfeO proteins have been grouped into five classes based on their domain architectures: class I, comprising a N-terminal cupredoxin-containing domain (Cup domain) and a C-terminal peptidase-M75 or imelysin-like domain; class II, comprising only a M75 domain (termed EfeM); class III, comprising an unidentified N-terminal domain and a M75 domain; class IV, comprising a class I EfeO fused to EfeU; and class V, comprising only a Cup domain (Rajasekaran et al. 2010). The Cup domain is posited to be involved in electron transfer and also has potential metal binding sites for Cu^{2+} and Fe^{3+}. Within the M75 domain is a conserved HXXE motif, a putative metal binding site through which iron could be transferred to EfeU (Rajasekaran et al. 2010), but the validity of this hypothesis remains unclear. More work will be necessary to understand the structure, function, and metal binding properties of EfeO to determine its role in the iron transport process.

12.3.4 Iron Transporter/More Regions Allowing Vacuolar Colocalization N Protein (IroT/MavN)

Legionella pneumophila is the causative agent of Legionnaires' disease, and when *L. pneumophila* infects host cells, it establishes a *Legionella*-containing vacuole (LCV) associated with the endoplasmic reticulum. Iron is required for the survival and virulence of intravacuolar pathogens, and IroT/MavN is a key transporter that functions at this location (Fig. 12.2, orange) (Portier et al. 2015; Isaac et al. 2015). A substrate of the intracellular *m*ultiplication/*d*efect in *o*rganelle *t*rafficking (Icm/Dot) type IV secretion system of the LCV, *mavN* is an iron-regulated gene encoding a 660 amino acid, 75 kDa protein that contributes to *Legionella* growth and iron transport in both amoeba and macrophages (Isaac et al. 2015; Portier et al. 2015; Christenson et al. 2019). Additionally, *L. pneumophila* bearing a non-functional MavN exhibited growth defects on iron-restricted agar and acquired Fe^{2+} at levels lower than wild type (WT) strains (Portier et al. 2015). These results indicate that MavN is important for iron acquisition to support the growth and the survival of this pathogen living within a variety of different environments.

Topologically, MavN is predicted to have 8 TM helices with both the N- and C-termini located in the cytoplasm. MavN also contains four predicted cytoplasmic loops and three predicted loops in the LCV lumen. This topology was verified by the transmembrane-substituted cysteine accessibility method (Christenson et al. 2019; Isaac et al. 2015). Like other iron-binding proteins, MavN also contains EXXE motifs and nine of these motifs can be found within the protein. An EXXE motif in a 70-amino acid loop (denoted at loop 7) mapped to the LCV lumen and conserved amongst all *Legionellaceae* species was the only one of these motifs determined to be wholly essential for *L. pneumophila* growth, as a plasmid carrying this mutation could not complement a Δ*mavN* growth defect (Isaac et al. 2015; Christenson et al. 2019). This loop also contains eight His residues, three of which were found to be important for MavN function in a triple mutant (Isaac et al. 2015). Only one His residue is predicted to be localized to the TM region along TM helix 6, and mutation of this residue exhibits a growth defect. Additionally, of the four Met residues in MavN, only one (along TM helix 3) led to a growth defect in vivo (Christenson et al. 2019). These in vivo results were subsequently used to test an in vitro transport model of MavN.

For in vitro analysis of MavN, the protein was heterologously expressed and purified from the methylotrophic yeast *Pichia pastoris*. Solubilization and purification in detergents $C_{12}E_6$ and $C_{12}E_8$ and yielded predominately dimeric protein (Christenson et al. 2019). To test substrate binding, Co^{2+} and Ni^{2+} were tested for their ability to bind to MavN as surrogates for Fe^{2+} under oxic conditions, and both substrates bound with modest affinity (K_d ca. μM) (Christenson et al. 2019). MavN was then reconstituted into a liposome to test for metal ion transport using calcein, a dye whose fluorescence is quenched by metal binding. Transport of several metal ions into proteoliposomes were tested and a K_M for Fe^{2+} transport was measured to be 16 μM. Though transport of Mn^{2+}, Co^{2+}, and Zn^{2+} into the proteoliposomes was

also observed, transport of Cu^{+}, Cu^{2+}, and Ni^{2+} was not (Christenson et al. 2019). To determine whether Mn^{2+} and Zn^{2+} could serve as substrates for MavN, these metals were provided in excess to a Δ*mavN* strain growing in bone marrow deficient macrophages, in addition to Fe^{2+}. In these experiments, both Mn^{2+} and Zn^{2+} stimulated growth of the Δ*mavN* strain, suggesting substrates other than Fe^{2+} could be translocated by MavN in vivo (Christenson et al. 2019). In vitro studies of Fe^{2+} transport into proteoliposomes with variant MavNs showed an importance for His and Met residues in Fe^{2+} translocation, while Cys variants only had modest effect on Fe^{2+} transport (Christenson et al. 2019).

Another study published shortly after also reconstituted MavN into liposomes for metal transport studies. In this study, MavN was heterologously expressed in *E. coli*, extracted from membranes with *n*-tetradecylphosphocholine (Fos-choline-14) and then purified in 7-cyclohexyl-1-heptyl-β-D-maltoside (Cymal-7), which resulted in chiefly monomeric protein (Abeyrathna et al. 2019). MavN was then incorporated into liposomes containing Fluozin-3, a turn-on fluorescent probe, to monitor transport activity. Transport of Fe^{2+} was monitored in an anoxic environment and similar K_d values (μM) were observed (Abeyrathna et al. 2019). However, contrary to the previous study, transport of Fe^{2+} was highly specific, and Co^{2+}, Ni^{2+}, and Zn^{2+} provided <5% of the Fe^{2+} response. As a control, Fe^{3+} was also tested for transport, and was not taken up by MavN. These results suggest that MavN could be highly specific for Fe^{2+} (Abeyrathna et al. 2019). Because of the acidic pH of the LCV, it was suggested that Fe^{2+} transport could be coupled to proton counter-transport. To test this, a pH indicator, pyranine, was incorporated into the proteoliposomes. Subsequently, as Fe^{2+} uptake occurred, the pH inside the vesicles increased, suggesting that MavN could function as an Fe^{2+}/H^{+} antiporter or as a secondary active transporter (Abeyrathna et al. 2019). To determine which residues may contribute to Fe^{2+} uptake, a series of variant proteins were constructed and incorporated into liposomes. A variant protein containing mutations to Glu and His residues in TM helices 2 and 3 and Asp and Cys residues in TM helix 8 was constructed and tested for transport. This variant maintained the same V_{max} as the WT protein; however, K_M was higher (>25 μM) (Abeyrathna et al. 2019). A different variant of Glu, Cys, and His residues at the TM-LCV interface abolished Fe^{2+} uptake, indicating that these residues could serve to release Fe^{2+} into the vacuole (Abeyrathna et al. 2019). Taken together, these in vitro assays to assess metal transport will be useful models for determining real-time metal transport of other transporters, especially for determining residues involved in the transport process. If used in conjunction with other biochemical and biophysical techniques, transport mechanisms could be determined, which could aid in the design of molecules that inhibit the transport process.

While the systems described above are known or are purported to be Fe^{2+} transport systems, they remain largely uncharacterized at both the cellular and the atomic levels. Furthermore, some of these transporters display a broad substrate specificity and they may have a relatively weak affinity for Fe^{2+}, at least under the tested experimental conditions. Additionally, some transporters such as ZupT do not appear to be broadly distributed amongst bacteria, though it is possible that

homologs have yet to be identified. The Efe system, though specific for Fe^{2+}, is only distributed in some pathogenic bacteria. To our knowledge, the only widespread, prokaryotic, Fe^{2+}-specific transport system to be identified and characterized in several organisms is the *ferro*us iron transport (Feo) system, which is described in detail below.

12.3.5 Ferrous Iron Transport by the Feo System

The Feo system is the predominant prokaryotic Fe^{2+} transport system (Fig. 12.2, purple). The *feo* operon, encoding for the Feo system, was first discovered in 1987 by isolating an *E. coli* strain defective for Fe^{2+} uptake (Hantke 1987). At that time, five *E. coli* Fe^{3+} transport systems for ferric siderophores had been identified, but no system had been identified for Fe^{2+} transport. The locus responsible for Fe^{2+} transport was then termed *feo*, but its position within the *E. coli* genome remained unknown at the time. Feo was subsequently identified to be a high affinity transporter, as cellular uptake studies revealed an apparent K_M of Fe^{2+} to be ≈0.5 μM, and in 1993, the *feoA* and *feoB* genes were cloned and their sequences were published (Kammler et al. 1993). The Feo system also appears to be under regulation by the *f*umarate and *n*itrate *r*eduction regulator (FNR) as FNR binding sites were found near the genes encoding for FeoA and FeoB (Fig. 12.4). FNR is a cAMP-like

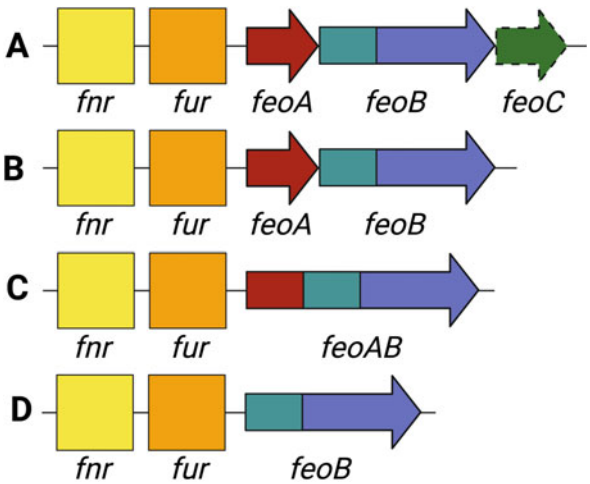

Fig. 12.4 The most common arrangements of the *feo* operon. (**a**) The operon encoding for FeoA, FeoB, and FeoC was first discovered in *E. coli* in 1987. However, the FeoC protein is poorly conserved (found in ≈13% of bacteria), which is denoted by a dashed line. These genes are downstream of the binding sites for the FNR and FUR regulators. (**b**) The most common operon arrangement encodes for only FeoA and FeoB. (**c**) Though rare, some *feo* operons encode for an FeoA-FeoB fusion, such as in *Bacteroides fragilis*. (**d**) Some *feo* operons encode for FeoB alone, demonstrating the essential nature of this gene. Figure created with BioRender

transcriptional regulator that senses oxygen using a [4Fe-4S] cluster and binds to DNA using a helix-turn-helix domain. The [4Fe-4S] cluster is degraded in the presence of oxygen, and this cluster change controls DNA binding and alters a metabolic "switch" that converts bacterial metabolism from anaerobic to aerobic respiration (Spiro and Guest 1990; Unden et al. 2002; Crack et al. 2008). Additionally, a FUR binding site (*f*erric *u*ptake *r*egulator, one of the master regulators of general prokaryotic iron metabolism) was also discovered downstream from the FNR binding site (Fig. 12.4) (Kammler et al. 1993). When cellular iron is low, the Fe^{2+}-FUR complex dissociates and allows for transcription of iron-responsive genes (Escolar et al. 1999; Troxell and Hassan 2013; Fillat 2014). Unsurprisingly, a *fur* mutant was observed to accumulate Fe^{2+} more rapidly than WT, indicating *feo* to be under FUR regulation. Thus, Feo-mediated Fe^{2+} transport is highly regulated, but whether additional levels of regulation exist for this system remains unclear.

As more genomic data have become available, it has been proposed that Feo represents an ancient Fe^{2+} transport system (Hantke 2003), which is supported by several lines of evidence. First, as previously described, it is clear that Fe^{2+} was the predominant species of iron present on Earth as bacteria first evolved, undoubtedly necessitating an Fe^{2+} uptake system. Second, several cyanobacterial descendants (among the first unicellular organisms to exist on the planet) retain an FeoB protein within their genomes, suggesting that this system has played a major role during their evolution to necessitate such prolonged genetic retention. In fact, this conservation suggests that despite the switch from an anoxic to a more oxygen-rich atmosphere, Fe^{2+} transport was still necessary for the survival of many organisms. FeoB may have co-evolved alongside organisms to supply metabolic feedstocks of Fe^{2+}, a strategy that is undoubtedly still operative on modern Earth. Underscoring this point is the major conservation and distribution of the *feo* operon across present-day bacterial species. As of 2003, it was estimated that ≈50% of all bacterial genomes that had been sequenced at that time contained an *feoB*-like gene (Hantke 2003), emphasizing the dominance of Feo in prokaryotic Fe^{2+} acquisition.

The organization of the tripartite *feoA*/*feoB*/*feoC* operon found in *E. coli* is considered to be canonical, as it was the first to be discovered (Fig. 12.4a) (Hantke 2003, 1987; Kammler et al. 1993). However, there are several other arrangements of the *feo* operon, and it is now clear that a tripartite system is unlikely to be the dominant arrangement in most sequenced prokaryotic genomes. The tripartite operon arrangement is predominantly found in the γ-proteobacteria class but can also be found in terrabacteria (Cartron et al. 2006; Lau et al. 2016; Sestok et al. 2018, 2021). The FeoA protein is most commonly found alongside FeoB and some operons are predicted to encode for multiple FeoA proteins (Fig. 12.4b) (Lau et al. 2016; Cartron et al. 2006; Sestok et al. 2018). A recent search of the FeoA protein (IPR007167) using the InterPro Database (accessed February 2021) revealed that ≈3% of all FeoA proteins exist as fusions of either two or three FeoA proteins (Sestok et al. 2021). FeoA can also exist as a naturally-occurring fusion to the N-terminal domain of FeoB (Fig. 12.4c) (Sestok et al. 2018; Lau et al. 2016; Veeranagouda et al. 2014; Rocha et al. 2019; Dashper et al. 2005); these fusions are rare, found predominantly in the *Bacteroidia* and *Clostridia* classes, and account

for only ≈8% of all FeoA-domain containing proteins in the InterPro Database (Sestok et al. 2021). Finally, some bacterial genomes encode for only FeoB (Fig. 12.4d).

Regardless of the arrangement of the organism's operon, it is clear that FeoB is the chief component of the Feo system based on its conservation (Fig. 12.4). FeoB is a complex, polytopic membrane protein thought to resemble a covalent fusion of a G-protein to that of a *G-p*rotein-*c*oupled *r*eceptor (GPCR). Guanine nucleotide-binding proteins, termed G-proteins, are a family of intracellular proteins and are associated with transmitting signals from external stimuli to the cell's interior. Each protein has two states, termed active and inactive, and for this reason G-proteins have been likened to molecular versions of switches. Consistent with this description, FeoB is typically composed of three main domains with their residues numbered relative to *E. coli* K-12 FeoB (Uniprot ID P33650): the G-protein domain that binds and hydrolyzes GTP (residues 1–170), the *g*uanine *d*issociation *i*nhibitor (GDI) domain (residues 171–276) that increases GDP affinity, and the TM region (residues 277–773) that has an ill-defined function. The G-protein domain and the GDI domain comprise the full N-terminal soluble domain of FeoB, which is termed NFeoB. To date, the majority of published literature on the Feo system has focused solely on NFeoB (vide infra), likely due to its more tractable, soluble form and its intriguing similarity to well-characterized G-proteins.

G-proteins play important roles in signal transduction in eukaryotic cells, but their roles in bacterial physiology are not well understood. In eukaryotes, G-proteins are numerous and as such are responsible for an array of cellular processes such as nuclear import and export, vesicle formation, exocytosis, regulation of the cytoskeleton, and cellular differentiation (Bos et al. 2007). In contrast, bacterial G-proteins may be involved in ribosome biogenesis, tRNA modification, cell cycle progression, or DNA replication. G-proteins cycle between on and off states, dependent on the identity of the nucleotide bound to the protein to carry out their molecular functions (Vetter and Wittinghofer 2001). GDP dissociation from a G-protein results in activation, which is followed by GTP binding and hydrolysis, returning the protein to its inactive form (Vetter and Wittinghofer 2001). Interestingly, bacterial G-proteins are structurally similar to eukaryotic G-proteins, but their nucleotide binding affinities are several orders of magnitude lower. Because eukaryotic GTPases display high nucleotide binding affinities and intrinsically slow GTP hydrolysis and GDP dissociation, *G-a*ctivating *p*roteins (GAPs) or *g*uanine *e*xchange *f*actors (GEFs) are needed either to increase the rate of GTP hydrolysis or to facilitate the release of GDP (Vetter and Wittinghofer 2001). Regions within the G-protein domain are also important for how guanine nucleotides are recognized, and how these proteins interact with downstream effectors. Conformational changes are observed in these regions (termed switch I and switch II), dependent upon the nucleotide-state of the G-protein (Bos et al. 2007; Vetter and Wittinghofer 2001). Many of these aspects have been explored with regards to NFeoB function, and an abbreviated synopsis is presented below.

Table 12.1 Consensus sequences for G-protein motifs in NFeoB. The G1–G4 motifs are conserved across bacterial taxonomic groups and were initially identified through multiple sequence alignments. The G5 motif was identified through structural alignments. All amino acid numberings are based on *Ec*FeoB

Motif	Position	Sequence	Role
G1	10–17	GXXXXGK(S/T)	Binds to α- and β-phosphate of GTP
G2	37	T	Binds to γ-phosphate of GTP and Mg^{2+}
G3	56–59	DXXG	Binds to γ-phosphate of GTP and Mg^{2+}
G4	120–123	NXXD	H-bonding to guanine nucleotide
G5	150–155	STRGRG	H-bonding to guanine nucleotide

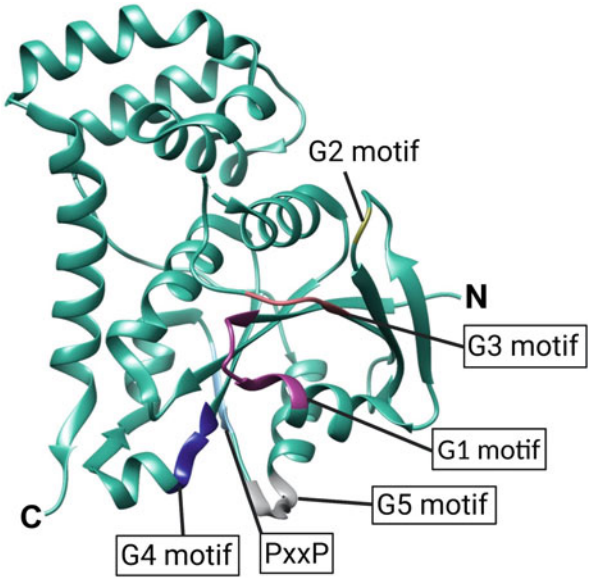

Fig. 12.5 X-ray crystal structure of *E. coli* NFeoB (PDB ID: 3I8S), comprising the GDI and G-protein domains. Five G-protein motifs are found in NFeoB and are responsible for the recognition and the binding of guanine nucleotides. The Pro-rich hydrophobic sequence in NFeoB is located along a β strand adjacent to the G5 motif and is believed to be the site of FeoA-FeoB interactions. 'N' and 'C' represent the N- and C-termini respectively. Figure created with BioRender

12.3.5.1 Composition and Structure of NFeoB

E. coli FeoB (*Ec*FeoB) was demonstrated to contain a G-protein domain in 2002, representing the first example of a G protein tethered to a prokaryotic membrane protein (Marlovits et al. 2002). At that time, >95 species containing FeoB homologs had been identified. There was (and still is) no predicted homology between the TM domain of FeoB and that of other transmembrane proteins (Marlovits et al. 2002). Using multiple sequence alignments, four of the five G-protein motifs were identified in *Ec*FeoB that are responsible for binding and hydrolyzing GTP (Table 12.1 and Fig. 12.5) (residues numbered based on *E. coli* K-12 FeoB; Uniprot ID P33650): G1 (residues 10–17; Fig. 12.5, purple), G2 (residue 37; Fig. 12.5, yellow), G3 (residues 56–59; Fig. 12.5, salmon) and G4 (residues 120–123; Fig. 12.5 blue). At

the time, the G5 motif (Fig. 12.5, gray) could not initially be identified because of poor sequence conservation (Marlovits et al. 2002).

In 2008, the linker region between the G-protein domain and the TM region in FeoB was identified as a GDI domain. Initially, a weakly-conserved LXXXE motif in the TM linker region identified by sequence alignments was believed to resemble a binding site for a GEF. An E210A variant was generated in both *Ec*NFeoB and full-length *Ec*FeoB. The *Ec*NFeoB^{E210A} variant exhibited a decreased 3′-*O*-(*N*-Methyl-anthraniloyl)-GTP (mant-GTP) affinity by approximately two-fold, but the mant-GDP affinity decreased by approximately four-fold. The authors attributed the function of the linker region between the G-protein domain and the TM region to that of a GDI domain instead of a GEF. The *Ec*FeoB^{E210A} variant was not functional in vivo, suggesting the GDI domain could play an important role in FeoB function (Eng et al. 2008). Subsequently, each domain was tested for the ability to affect nucleotide binding affinities. The presence of the GDI domain increased the affinity of mant-GDP by 13-fold, and the presence of the TM region further increased the affinity for mant-GDP by 400-fold. The binding affinity for mant-GTP by the G-protein domain and NFeoB were similar; however, the full-length *Ec*FeoB exhibited much stronger binding of mant-GTP, further demonstrating that this region functions as a GDI domain (Eng et al. 2008). Interestingly, multiple sequence alignments of the NFeoB domains from *E. coli*, *Salmonella typhimurium*, *Vibrio cholerae*, and *Helicobacter pylori* showed that the linker region varies in sequence and length, which could be a functional variation among species for this domain. Subsequent structural analyses then provided further insight into this intriguing domain.

Some of the first structures of the G-protein domain of FeoB (residues 1–184) were determined in 2009 from the archaeon *Methanococcus jannaschii* in the apo (PDB ID: 2WJH), GDP-bound (PDB ID: 2WJG), and GMP-PNP bound (PDB ID: 2WJI) forms (Koster et al. 2009a, b). *M. jannaschii* NFeoB (*Mj*NFeoB) crystallized as a homodimer in the presence and absence of nucleotides, in which the nucleotide binding pockets form the dimeric interface. The overall structure of *Mj*NFeoB revealed six α-helices and a core β-sheet composed of seven β-strands. However, major structural differences exist in the G-domain dependent upon the nucleotide state of the protein. In the GTP-bound form, the Switch I loop points away from the nucleotide binding site and the β-sheet in the GTP-bound form lacks one β-strand (residues 32–36), which could not be seen in the electron density. This suggests that the Switch I loop, located between the G1 and G2 motif, may be more flexible in the GTP-bound form. Additionally, structural alignments of *Mj*NFeoB with eukaryotic GTPases revealed the G5 motif, not previously identified through sequence alignments, to be located at position 145–148 (SAAK) (Koster et al. 2009b).

The *Streptococcus thermophilus* NFeoB was crystallized in the presence of $GDP{\cdot}AlF_4^-$, a transition-state analog that locks the G-protein in its active state, providing insight into how GTP hydrolysis is initiated (Ash et al. 2011). *St*NFeoB was co-crystallized with $GDP{\cdot}AlF_4^-$, one K^+ ion, and one Mg^{2+} ion (PDB ID: 3SS8) (Ash et al. 2011). This transition-state structure of *St*NFeoB captured the Switch II region pointing away from the nucleotide binding site, in contrast with the Switch I

region that caps the nucleotide binding site, as observed in the previous mant-GMP-PNP bound structures (Ash et al. 2011). The K^+ ion is bound in the nucleotide binding site with coordination by Gly29, Trp31, and Asn11, similar to its position in 3LX5, while the Mg^{2+} ion, ≈5 Å away from the K^+, contacts the planar AlF_4^- molecule that mimics the γ-phosphate of the nucleotide. Additional AlF_4^- interactions include an oxygen atom from the β-phosphate, backbone amides from Gly33, Val34, and Thr35 in the Switch I region, and a water molecule that performs nucleophilic attack (Ash et al. 2011). Importantly, the attacking water appears to be solvent exposed in this structure, which could allow the positioning of another catalytic residue, possibly from a different domain in FeoB or another partner protein (Ash et al. 2011).

In 2013, the X-ray crystal structure of NFeoB from *Gallionella capsiferriformans* was published in both the apo and the GDP-bound states. *G. capsiferriformans* provides a unique look into the structure of the cytoplasmic domain of FeoB, as *Gc*FeoB lacks a GDI domain while the G-protein domain is structurally analogous to that of *Ec*NFeoB (PDB ID: 3HYT) (Deshpande et al. 2013). While *Gc*NFeoB was chiefly monomeric in solution, the protein crystallized as a domain-swapped dimer (Deshpande et al. 2013). *Gc*NFeoB also contained the five G-protein motifs but exhibited a highly disordered G5 motif in both the apo structure and the GDP-bound structure (Deshpande et al. 2013). In agreement with the crystal structure of *S. thermophilus* NFeoB, the Switch I region was oriented away from the GDP binding pocket, supporting the hypothesis that the Switch I region is necessary for nucleotide binding and release (Deshpande et al. 2013).

Another crystal structure of NFeoB from *E. coli* BL21 was solved in 2016 (Hagelueken et al. 2016). After removal of the nucleotide, which typically co-purified with the protein, *Ec*NFeoB crystallized as a trimer. This structure was similar to other apo NFeoB structures with the switch I region pointing away from the nucleotide binding site (suggested to be in the "open" conformation) (Hagelueken et al. 2016).

Numerous X-ray crystal structures of variant NFeoBs from several organisms have since been solved. However, these structures have failed to answer questions about how the Switch I and Switch II regions may be involved in regulating nucleotide binding and release, Fe^{2+} transport, and potential protein-protein interactions. Likewise, structural changes that might occur in the GDI domain upon metal binding and release have not been determined because FeoB lacks the TM region, further underscoring the importance of undertaking structural studies of full-length FeoB.

12.3.5.2 NFeoB Function and GTPase/NTPase Activity

Early seminal results revealed the ability of NFeoB to bind guanine nucleotides, and experiments have importantly linked the activity of the G-protein domain to Fe^{2+} uptake. Stopped-flow studies of *Ec*NFeoB with non-hydrolyzable guanine and adenine nucleotide analogs, mant-5′-Guanylyl-imidodiphosphate (mant-GMP-

PNP) and mant-5′-Adenylyl-imidodiphosphate (mant-AMP-PNP), revealed specificity towards guanine nucleotides (Marlovits et al. 2002). At 20 °C, the K_d of affinity-tagged *Ec*NFeoB for mant-GMP-PNP was determined to be ≈4 μM (based on slow association but fast release kinetics), similar to Era but three orders of magnitude lower than p-21 Ras (Marlovits et al. 2002). However, a follow-up study of *Ec*NFeoB measured a K_d for mant-GTP to be 12 μM, a threefold increase over what was previously observed for mant-GMP-PMP, suggesting the non-hydrolyzable analog may not be a good proxy for GTP binding (Eng et al. 2008). GTP hydrolysis of *Ec*NFeoB was markedly slow at ≈0.0015 s^{-1} and hydrolysis of ATP was not observed (Marlovits et al. 2002). Initially, two potential sites existed for the G4 motif, residues 91–94 or residues 120–123. To determine which site contained the G4 motif, two variants (D94N and D123N) were tested for their ability to bind mant-GMP-PNP in stopped-flow experiments and only the D94N variant could bind mant-GMP-PNP, confirming the G4 motif is located at positions 120–123 (Marlovits et al. 2002). Because the D123N variant failed to recognize mant-GMP-PNP, it was suggested that D123 could impact Fe^{2+} transport in the full-length protein. In an *feoB* deletion strain deficient for Fe^{2+} uptake, full-length FeoB was able to rescue Fe^{2+} uptake whereas a plasmid carrying a D123N variant was not. These results thus demonstrated a link between GTP binding, GTP hydrolysis, and Fe^{2+} transport (Marlovits et al. 2002).

Following these results, biochemical and structural experiments have revealed the contributions of some G motifs (and G5 in particular) to NFeoB-catalyzed GTP hydrolysis. Eight *Ec*NFeoB variants located in the G motifs and switch regions, were examined for their effects on nucleotide binding and *feoB* function in vivo. All variants exhibited at least a two-fold decrease in GDP affinity, while only a T37A variant drastically decreased GTP affinity and could not restore Fe^{2+} uptake in a *feoB*-deficient strain (Eng et al. 2008). The N32A and D73A variants were able to hydrolyze GTP, but could not restore Fe^{2+} transport in a *feoB*-deficient strain (Eng et al. 2008). Additionally, the P12G, T60Q, and Y61A variants restored in vivo function of FeoB while the Y61E and P58A variants did not (Eng et al. 2008). Another study on *Ec*NFeoB investigated changes in GDP release as a result of differences in sequence composition in the G5 motif (Álvarez-Fraga et al. 2018). Structural changes in the G5 motif are common in GTPases, but the NFeoB G5 motif seems to have poor sequence conservation and consists of six amino acids (V149–G154). In several structures of NFeoB, the loop formed by the G5 motif interacts with nucleotides through a mixture of H-bonding and hydrophobic interactions between the polypeptide and the nucleotide base (Álvarez-Fraga et al. 2018). This interaction must be important, as this structural motif is conserved despite low sequence conservation. An alanine in the second position in the G5 motif is typically the most conserved residue, and mutation of this analogous residue in eukaryotic GTPases results in severe health complications (GDP is released so fast the protein is always "on") (Álvarez-Fraga et al. 2018). Interestingly, *E. coli* FeoB does not conserve an alanine residue, but rather a serine residue in this position. For WT *Ec*NFeoB, GTPase activity was measured at 0.40 min^{-1} in the presence of K^+, a sevenfold increase than in the presence of Na^+ (Álvarez-Fraga et al. 2018).

Subsequently, each residue was separately mutated to an alanine. All variants, with the exception of a S150A variant, displayed lower GTPase activity. The S150A variant's GTPase activity was 1.5-fold faster than the WT protein and exhibited a seven-fold slower release rate of mant-GDP (Guilfoyle et al. 2014). Using ITC, the S150A variant bound GDP five-fold higher than the WT, which correlates well with an observed slower GDP release (Álvarez-Fraga et al. 2018). Interestingly, differences in nucleotide binding and release are attributed to alterations in the hydrogen bonding network to the nucleotide base when serine is present versus alanine, destabilizing the nucleotide base. While the sequence composition of the G5 loop is clearly important for nucleotide binding and release, it remains unknown whether GDP release is a result of loop movement or if loop movement is a result of GDP release (Álvarez-Fraga et al. 2018).

Despite structural homology to eukaryotic G-proteins, recent publications have suggested that some FeoB proteins may be NTPases rather than strict GTPases. The first study to explore this idea found that *Vc*NFeoB could hydrolyze both GTP and ATP, with a preference for GTP over ATP. Interestingly, *Vc*NFeoB was also able to hydrolyze inosine triphosphate (ITP), but saturating conditions were never achieved. In contrast, *Ec*NFeoB hydrolyzed GTP and ITP but did not hydrolyze ATP (Shin et al. 2019). Two variants in the G5 motif (S148T and N150T), which are responsible for interactions with the nucleotide base, displayed decreased ATPase activity but were able to transport Fe^{2+} in vivo, suggesting the variant *Vc*NFeoBs were functional GTPases but not functional NTPases (Shin et al. 2019). *Helicobacter pylori* NFeoB was also tested for NTPase activity in this study and was able to hydrolyze GTP, ITP, and ATP, thus leading to the classification of *Hp*NFeoB as an NTPase (Shin et al. 2019). *Vc*FeoA and *Vc*FeoC were also tested for their effects on GTPase and ATPase activity of *Vc*NFeoB. When *Vc*FeoA and *Vc*NFeoB were mixed at a 1:1 ratio in the presence of 650 μM ATP, ATP hydrolysis was reduced by ≈60%, and the addition of *Vc*FeoC at a 2:1:2 ratio did not have any further effect on ATPase activity. Conversely, *Vc*FeoA and *Vc*FeoC stimulated GTPase activity of *Vc*NFeoB at a 2:1:2 ratio. These results suggest that, at least in *V. cholerae*, FeoA and FeoC could function to regulate nucleotide hydrolysis activity (Shin et al. 2019). These observations raise interesting questions about the roles of FeoA and FeoC and whether their functions differ depending on whether their cognate FeoBs are strict GTPases or promiscuous NTPases.

A follow-up study further characterized NFeoB proteins from different organisms and suggested a sequence dependence on GTPase/NTPase classification (Shin et al. 2020). The authors found that NFeoBs from *E. coli*, *Salmonella enterica* serovar Typhimurium, and *Pseudomonas aeruginosa* (all Gram-negative pathogens) were only capable of hydrolyzing GTP, whereas NFeoBs from *Streptococcus mutans, Staphylococcus aureus,* and *Bacillus cereus* (all Gram-positive pathogens) were able to utilize both GTP and ATP (Shin et al. 2020). Through the use of multiple sequence alignments, the presence of a serine or alanine at position 150 (in *Ec*NFeoB) was used to predict whether a NFeoB protein would be a GTPase or an NTPase, respectively. Phylogenetic analysis showed that NFeoB proteins with GTPase activity and the conserved Ser appear to be clustered together and

predominantly present in γ-proteobacteria, with the exception of *V. cholerae* and *H. pylori*, while those with NTPase activity and the conserved Ala are broadly distributed in different phyla (Shin et al. 2020). All WT NFeoBs displayed increased GTP and ATP hydrolysis with increasing temperature. Interestingly, *Bc*NFeoB displayed a preference for ATP at lower temperatures and GTP at higher temperatures (Shin et al. 2020). Why some FeoB proteins would potentially favor dual nucleotide specificity and some would favor GTP as a substrate remains unknown, and further studies investigating nucleotide binding and hydrolysis in full-length FeoBs will be necessary to determine dual nucleotide specificity.

While several NFeoBs have been structurally characterized throughout the GTP-hydrolysis cycle, there has been much debate regarding the functional oligomeric state of NFeoB (and thus full-length FeoB) in vivo. Q-band *p*ulsed *el*ectron-electron *do*uble *r*esonance (PELDOR) spectroscopy was used to characterize conformational, dynamical, and oligomeric changes in *Ec*NFeoB in the presence and absence of GTP. These data demonstrated that the largest structural changes in NFeoB during GTP binding occur in the switch I region (Hagelueken et al. 2016). A doubly MTSSL spin labelled but apo (nucleotide-free) *Ec*NFeoB was found to adopt an "open" conformation in solution (≈40 Å label distance), similar to that seen in the crystal structure of *Ec*NFeoB. The addition of a 20-fold molar excess of GTP or GDP decreased the distance distribution of the spin labels on the protein to ≈20 Å, which was attributed to the "closed" state of the protein in which the switch I region moves to cover the GTP binding pocket, similar to the PELDOR observations (Hagelueken et al. 2016). This experiment was repeated with a 100-fold molar excess of GMP-PNP, which induced a conformational change from the "open" state to the "closed" states; however, this shift only corresponded to ≈5% of *Ec*NFeoB molecules in the "closed" state (Hagelueken et al. 2016). While the presence of K^+ did stimulate GTP hydrolysis activity of *Ec*NFeoB, the presence of K^+ did not affect the conformation of the switch I region (Hagelueken et al. 2016). A K1 spin label was then incorporated into *Ec*NFeoB to investigate oligomeric states present in solution. At low concentrations (25 μM), *Ec*NFeoB was found to be monomeric in solution, but ≈5% of *Ec*NFeoB molecules formed higher-order oligomers at much higher protein concentrations (≈500 μM). While the data suggest *Ec*NFeoB monomers could interact at high concentrations, the authors noted that these interactions do not appear to be specific as the distance distribution observed was broad (Hagelueken et al. 2016). Thus, the exact oligomerization of the soluble NFeoB domain remains an open debate.

12.3.5.3 Full-Length FeoB

An intellectually curious aspect of FeoB is its unique combination of a G-protein covalently attached to a large TM region, resembling a hybrid of strategies commonplace in nature. Typically, small G-proteins cycle between active (GTP-bound) and inactive (GDP-bound) conformations depending on the nucleotide status of the protein and the cell (Bos et al. 2007). To assist localization of G-proteins to the

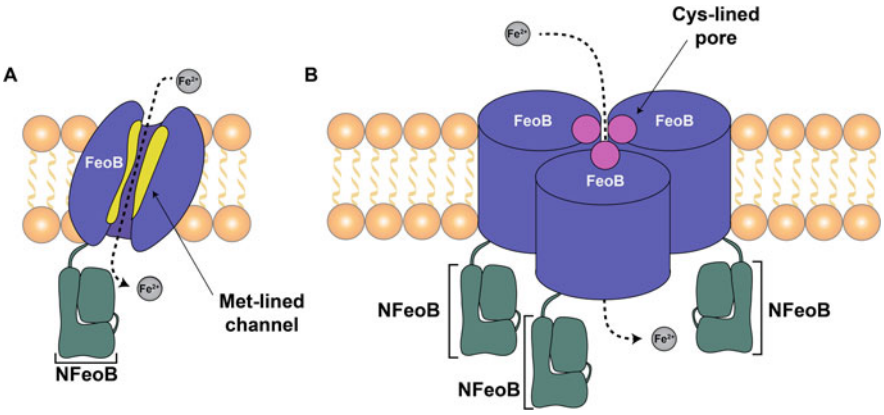

Fig. 12.6 Models of FeoB-mediated Fe^{2+} transport. (**a**) Our laboratory has proposed that FeoB utilizes a Met-lined channel (yellow) to bind and to transport ferrous iron across the bacterial membrane (Sestok et al. 2018) based on a de novo calculated model of *Ec*FeoB (Ovchinnikov et al. 2017). (**b**) Others have proposed that FeoB utilizes an oligomerically-induced Cys-lined pore (pink) to bind and to transport Fe^{2+} across the bacterial membrane based on a model of *Pa*FeoB that has modest sequence homology to several functionally different bacterial transporters (Seyedmohammad et al. 2016)

membrane, their C- and/or N-termini may be prenylated, myristoylated, or acetylated (Bos et al. 2007). GDI domain-lipid tail interactions allow for G-proteins to be removed from the membrane and provide another level of control over G-proteins, in addition to GAPs and GEFs. GDI domain regulation in G-proteins is common in Rho and Rab GTPases (Bos et al. 2007). In the case of FeoB, the G-protein domain is uniquely tethered to its TM region by a GDI domain. It could be possible that interactions between the GDI domain and the TM region provide control over nucleotide binding at the G-protein domain, nucleotide hydrolysis, and even Fe^{2+} transport. However, structural and functional studies on FeoB are scarce, representing a major hole in our understanding of this component of the Feo system.

While no structure of an intact FeoB exists, the first model to appear was that of *Pseudomonas aeruginosa* FeoB (*Pa*FeoB) (Fig. 12.6). In this model, the predicted structure of the N-terminal domain was based on homology to the crystal structure of *Ec*NFeoB (crystallized as a trimer in the presence of mant-GTP; PDB ID: 3HYT) (Seyedmohammad et al. 2016). The TM region of FeoB was then modelled based on sequence similarity to an archaeal glutamate transporter (crystallized as a trimer; PDB ID: 1XFH). The linker region responsible for joining the soluble *Pa*NFeoB domain with the TM region was modelled based on sequence identity to the EDH2 ATPase (crystallized as a dimer; PDB ID: 2QPT), and the C-terminal domain of *Pa*FeoB was modelled based on sequence identity to dihydrodipicolinate reductase (crystallized as a tetramer; PDB ID: 1DIH) (Seyedmohammad et al. 2016). Despite these oligomeric discrepancies, the entirety of the *Pa*FeoB polypeptide was modelled as a homotrimer, and two conserved cysteine residues in *Pa*FeoB were suggested to be involved in the binding and transport of Fe^{2+} (Fig. 12.6). Blue native

PAGE and atomic force microscopy of purified *Pa*FeoB in $C_{12}E_8$ revealed three oligomeric states to be present: monomer, trimer, and hexamer. Based on the available data, monomeric *Pa*FeoB seems to be the predominant oligomeric state followed by trimeric *Pa*FeoB, with hexameric *Pa*FeoB being the least prevalent (Seyedmohammad et al. 2016). A putative metal-binding residue Cys^{429}, topographically modeled to be in TM helix 4, is predicted to form a ring within the homotrimer model. With an estimated diameter of ≈5 Å, this pore is hypothesized to be in the "open" state of the protein, which would be capable of transporting Fe^{2+} (Seyedmohammad et al. 2016). To probe this hypothesis further, GTPase activity of WT and variant *Pa*FeoBs was measured and tested for stimulation by Fe^{2+}. Maximal stimulation of GTPase activity occurred in the presence of 1–1.5 mM Fe^{2+}. Furthermore, a C429S variant had no effect on GTPase activity while a C675S variant, topographically modeled to be in TM helix 7 and predicted to be exposed to the periplasmic space, significantly reduced GTPase activity. The authors thus rationalized that Cys^{675} could serve as an Fe^{2+} sensor (Seyedmohammad et al. 2016). While this model provides one starting place for biochemical experiments to probe the mechanism of FeoB-mediated Fe^{2+} transport, another model exists that suggests a different transport mechanism could be possible.

A second model, this time of *E. coli* FeoB, was published in 2017 (Fig. 12.6) (Ovchinnikov et al. 2017). There are no true homologs of full-length FeoB and, because of its large size, accurate de novo models have been difficult to generate. Unlike the *Pa*FeoB model, which was created by using proteins with modest sequence similarity to *Pa*FeoB, the *Ec*FeoB model was generated by determining residue-residue contacts with metagenome sequence data. This combination of evolutionary data and structural prediction has resulted in the generation of hundreds of structures of proteins from families without previously known structures (Ovchinnikov et al. 2017). Analysis of the de novo *Ec*FeoB, a monomeric structure, reveals within FeoB the presence of a Met-lined channel that could serve as a translocation pathway for Fe^{2+} (Fig. 12.6) (Sestok et al. 2018). Additionally, the Cys residue predicted to be located at the periplasmic face and involved in the formation of a Cys-lined pore in the *Pa*FeoB model (Cys^{675}) is located within the TM region in the *Ec*FeoB model (Cys^{677}) (Sestok et al. 2018). However, despite the presence of two FeoB models, neither has been validated, and a full-length structure of FeoB is still unrealized, likely due to the difficulty of working with the intact membrane protein.

Despite the lack of atomic-level details of FeoB, at least a few publications have aimed to broaden our understanding of FeoB by addressing the challenge of large-scale expression and purification of the intact protein. In 2014, full-length *Pa*FeoB and a D123N variant were the first particulate FeoB constructs to be solubilized in *n*-dodecyl-β-D-maltoside (DDM) micelles, to be purified, and to be characterized functionally in vitro. Unstimulated GTP hydrolysis was slow (≈0.0035 s^{-1}), in agreement with the slow hydrolysis rates measured for soluble NFeoB. GTP hydrolysis by the D123N variant (a key G4 motif) was modestly altered to ≈0.0012 s^{-1}, demonstrating the importance of this residue in the full-length protein (Seyedmohammad et al. 2014). Functional reconstitution of *Pa*FeoB into

inside-out vesicles was also performed, and the GTP hydrolysis was modestly increased to ≈0.0046 s^{-1} in the absence of any metal or additional proteins (Seyedmohammad et al. 2014). In 2015, full-length *Ec*FeoB and N-terminal *Ec*NFeoB were both expressed and purified for spin-labelling EPR studies. An unnatural amino acid, *para*-acetylphenylalanine (pAcF), was incorporated into full-length *Ec*FeoB at Lys^{127} for this purpose (Hagelueken et al. 2015). Labeled *Ec*FeoB was subsequently solubilized and purified in DDM. The dominant sizing profile of purified *Ec*FeoB corresponded to a molecular weight of ≈480 kDa, while EPR experiments used rotational constants of the spin label to estimate the size of *Ec*FeoB at ≈300 kDa. The results suggest that *Ec*FeoB can form higher-order oligomers under these conditions (Hagelueken et al. 2015). However, spin labelled, full-length *Ec*FeoB solubilized in DDM or incorporated into 3-([3-Cholamidopropyl]dimethylammonio)-2-hydroxy-1-propanesulfonate/dipalmitoylphosphatidylcholine (CHAPSO/DMPC) bicelles did not appear to form higher order oligomers based on PELDOR experiments. These results were confirmed by mass spectrometry and negative-stain electron microscopy (Hagelueken et al. 2016). Thus, the in vitro oligomerization of *Ec*FeoB remains an open debate.

In 2018, expression, solubilization, and purification of full-length *Klebsiella pneumoniae* FeoB in DDM and $C_{12}E_8$ was the first in vitro study of this construct. In contrast to previous studies that measured the GTP hydrolysis rates of *Kp*NFeoB alone, GTP hydrolysis of full-length *Kp*FeoB was determined to be orders of magnitude higher at ≈0.09 s^{-1} for the DDM-solubilized protein and ≈0.03 s^{-1} for the $C_{12}E_8$-solubilized protein (Smith and Sestok 2018). The stimulation of GTP hydrolysis by exogenous potassium was not observed, in contrast to *Kp*NFeoB. Intriguingly, given the rapid rate of basal GTP hydrolysis, these observations suggest that the TM region of FeoB is able to significantly increase GTP hydrolysis levels, which could be operative for active transport. Whether FeoB transports Fe^{2+} in a facilitated or active manner remains an open debate. Additional factors that could stimulate GTP hydrolysis further, such as protein-membrane or protein-protein interactions, have yet to be identified (Smith and Sestok 2018). This paucity of information on the intact, full-length protein further emphasizes the need for additional biophysical and biochemical studies of intact FeoB.

12.3.5.4 FeoA

Within the *feo* operon, *feoA* is the most common gene appearing alongside *feoB* (Lau et al. 2013), suggesting FeoA plays an important role in Fe^{2+} uptake. FeoA is a small, cytoplasmic, β-barrel protein (Fig. 12.7) of approximately 8 kDa chiefly composed of a Src Homology 3-Like (SH3) domain. SH3 proteins fold to form a hydrophobic core, with the β-sandwich held together by three loops termed the RT-Src loop, the N-Src loop, and the distal loop. The RT-Src loop and the N-Src loop contribute to peptide binding while the distal loop contributes to ligand binding (D'Aquino and Ringe 2003; Li 2005). In eukaryotes, SH3 domains have been implicated in a suite of signal transduction mechanisms, facilitating protein-protein

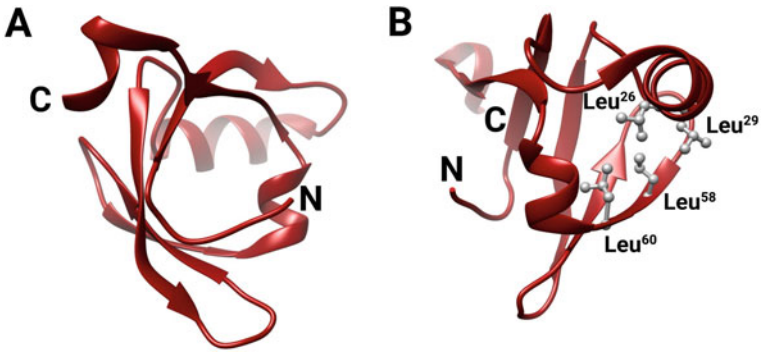

Fig. 12.7 X-ray crystal structure of *Kp*FeoA (PDB ID: 6E55). (**a**) FeoA is a β-barrel protein composed of an SH3-like domain. (**b**) FeoA contains a hydrophobic clamp with Leu resides (displayed in gray) postulated to be involved in protein-protein interactions with the N-terminal domain of FeoB. Panel **b** is displayed as a 90° vertical rotation relative to Panel **a**. 'N' and 'C' represent the N- and C-termini respectively. Figure created with BioRender

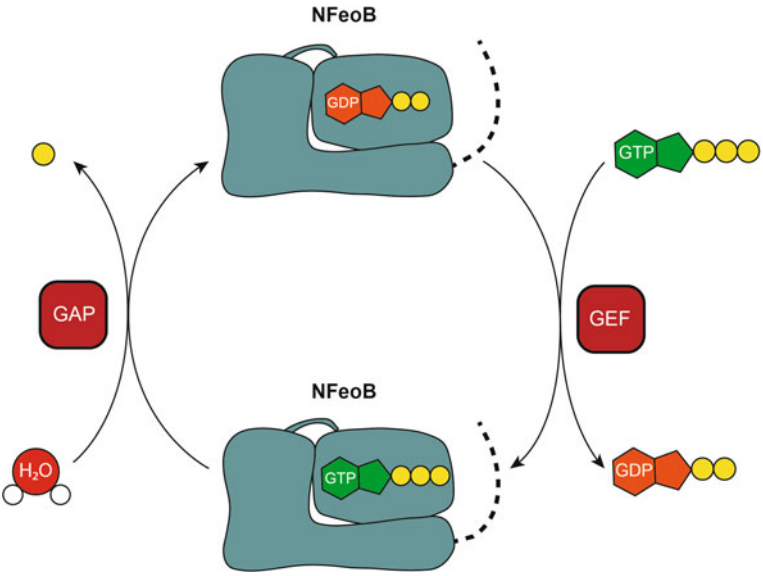

Fig. 12.8 Cartoon representing two possible functions of FeoA (red polygon) with respect to NFeoB (teal polygon). FeoA has been speculated to act as either a GTPase activating protein (GAP), which facilitates GTP hydrolysis to GDP in order to turn "off" function, or as a guanine exchange factor (GEF), which facilitates exchange of bound GDP for GTP in order to turn "on" function

interactions by interacting with their binding partners through a Pro-rich region that typically folds into a left-handed helical conformation (D'Aquino and Ringe 2003; Li 2005). SH3 proteins were initially believed to be absent from prokaryotes, but

have since been discovered while remaining widely uncharacterized (D'Aquino and Ringe 2003). Structures of FeoA from different organisms have been determined, yet the function of FeoA still remains unknown. Two plausible roles for FeoA include functioning as either a GEF or as a GAP (Fig. 12.8). In eukaryotes, GEFs and GAPs are crucial regulatory proteins that participate in the nucleotide cycling of G-proteins and provide signaling specificity (Bos et al. 2007; Vetter and Wittinghofer 2001). GEFs function by physically removing GDP bound to G-proteins via protein-protein interactions, allowing for GTP subsequently to bind to the apo G-protein (turning the signal from "off" to "on"). Conversely, GAPs function by catalyzing the hydrolysis of GTP to GDP, most commonly by intercalating a positively-charged residue on the GAP (such as Arg and Lys) into the GTP-binding site on the G-protein, increasing the polarization rate of the GTP phosphoester bond (turning the signal from "on" to "off") (Fig. 12.8) (Bos et al. 2007; Vetter and Wittinghofer 2001). Whether FeoA functions as a GEF or GAP remains to be seen, but the structure of FeoA strongly suggests its involvement in protein-protein interactions.

While several unpublished NMR structures of the FeoA SH3-like domain appeared in the PDB (*Protein Data Bank*) in the early 2000s (*P. aeruginosa* FeoA PDB ID: 2H3J; *K. pneumoniae* FeoA PDB ID: 2GCX; and *Clostridium thermocellum* FeoA PDB ID: 2K5L) the first published X-ray structure of FeoA appeared in 2010 from *Stenotrophomonas maltophilia* (PDB ID: 3MXH) (Su et al. 2010). The structure was determined to 1.7 Å resolution and contained two molecules in the asymmetric unit. Both molecules of FeoA adopted a SH3-like fold, as seen in the previous, unpublished NMR structures (Su et al. 2010). The SH3-like fold in FeoA is chiefly composed of 5 β-strands linked together through the RT-loop, the N-Src-loop, and α-helices (Fig. 12.7). One intriguing aspect of the *Sm*FeoA structure is the presence of two zinc ions and six chloride ions, which the authors attribute to the facilitation of *Sm*FeoA oligomerization (Su et al. 2010). The second published structure of FeoA was an NMR structure of *Ec*FeoA (Lau et al. 2013). Similar to *Sm*FeoA, *Ec*FeoA comprises two antiparallel β-sheets that form the β-barrel, and unstructured loop regions. However, *Sm*FeoA contains three α-helices whereas *Ec*FeoA only contains 2 α-helices (Lau et al. 2013; Su et al. 2010). These small, structural differences could be the result of low sequence conservation between *Sm*FeoA and *Ec*FeoA, while *Ec*FeoA and *Kp*FeoA have high sequence identity (90%) and are more structurally similar (Lau et al. 2013; Su et al. 2010). Finally, a recent X-ray crystal structure of *Kp*FeoA (PDB ID: 6E55) was determined to 1.5 Å resolution. Noteworthy was the observation of FeoA-FeoA interactions, which were speculated to be the location for FeoA-NFeoB interactions. Two sets of *Kp*FeoA dimers were present in the asymmetric unit and participate in unique FeoA-FeoA interactions at the dimer interface via intercalation of hydrophobic Leu residues (Fig. 12.7b) from one *Kp*FeoA molecule with Ala residues on the second *Kp*FeoA molecule (Linkous et al. 2019). When compared to an unpublished NMR structure of *Kp*FeoA (PDB ID: 2GCX), there is an ≈4 Å closure in the clamp. This crystallographic *Kp*FeoA is believed to represent the "closed" state while the FeoA present in the NMR structure is believed to represent the "open" state. In silico docking experiments using a 10 amino acid sequence from *Kp*FeoB containing the

PXXP motif revealed that the 10-mer could bind in the "open" *Kp*FeoA model. Strikingly, the 10-mer was predicted to bind within the "C-shaped" clamp (Fig. 12.7b), similar to where the FeoA-FeoA interactions occur, but only in the "open" form of the model. It is thus possible that FeoA interacts with FeoB at the PXXP site via the hydrophobic residues in the clamp region and could alter the nucleotide status of the G-protein domain by increasing GTP hydrolysis or facilitating GDP release thus regulating Fe^{2+} uptake via FeoB (Linkous et al. 2019). However, these structures alone are insufficient to determine the function of FeoA and more research will be necessary to determine the nature of the interaction between FeoA and FeoB and whether these hydrophobic residues are necessary to mediate the interaction.

Despite the availability of several FeoA structures revealing an SH3-like fold, the function of FeoA remains unknown and is of debate. Unlike eukaryotic SH3 domains, prokaryotic SH3 domains are not as well characterized. The presence of the SH3-like domain suggests that FeoA could be involved in protein-protein interactions, likely with FeoB as suggested by the *Kp*FeoA structure. However, while some studies have tried to establish the function of FeoA little information exists about FeoA-FeoB interactions at the protein level. One study explored the effect of *Ec*FeoA on the GTP hydrolysis activity of *Ec*NFeoB by using NMR to monitor ^{31}P signals indicative of GTP hydrolysis (Lau et al. 2013). In the presence of equimolar amounts of *Ec*FeoA, *Ec*NFeoB did not exhibit any obvious changes in GTPase activity, leading to the conclusion that FeoA does not act as a GAP on NFeoB alone (Lau et al. 2013). However, the effect of FeoA on intact FeoB is still unknown and higher stoichiometric ratios of FeoA:FeoB may be necessary for activity. More studies will ultimately be necessary to determine if FeoA has any effect on GTP hydrolysis, GDP release, and/or Fe^{2+} transport.

12.3.5.5 FeoAB Fusions

Some *feo* operons encode for a single polypeptide in which FeoA is naturally fused to the N-terminal soluble domain of FeoB. While these fusions are rare in genomic distribution, these observations further support the hypothesis that FeoA and FeoB are meant to interact physically to affect function. While these fusions are not well studied, they appear in the genomes of some very common human pathogens, such as *Porphyromonas gingivalis* and *Bacteroides fragilis*. Work on these fusions has chiefly been done at the cellular level (vide infra); unfortunately, no work at the protein level has examined these proteins.

12.3.5.6 FeoC

FeoC is a small protein of unknown function encoded along the *feoC* portion of the *feo* operon (Fig. 12.9). Unlike the strongly conserved *feoA* gene, *feoC* is thought to be present in only ≈13% of *feo* operons, predominantly in γ-proteobacteria (Lau

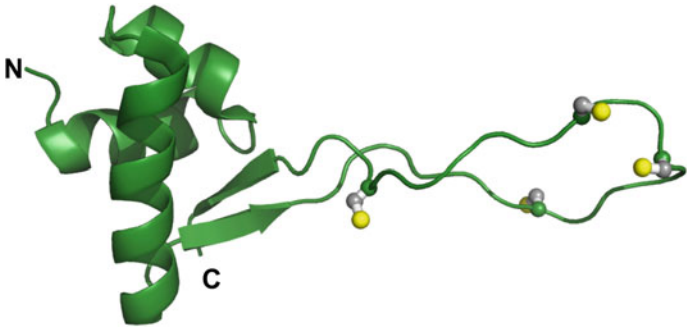

Fig. 12.9 Lowest-energy NMR conformer of *E. coli* FeoC (PDB ID: 1XN7). Displayed in gray and yellow are the highly-conserved Cys residue sidechains that are involved in coordination of the [Fe-S] cluster. Labels 'N' and 'C' represent the N- and C-termini, respectively

et al. 2013). The solution NMR structure of monomeric *Kp*FeoC (PDB ID: 2K02) was the first to be described and demonstrated that FeoC contains an N-terminal helical domain and a C-terminal unstructured loop, which combined are reminiscent of a winged-helix domain (Fig. 12.9) (Hung et al. 2012a). It has therefore been suggested that FeoC could serve as a transcriptional regulator (Cartron et al. 2006). However, upon comparison of the protein electrostatics of *Kp*FeoC to that of other DNA binding proteins, such as DtxR and the DNA binding domain of BlaI, it has been noted that the corresponding helix in *Kp*FeoC is very negatively charged and therefore would not favor an interaction with DNA based on electrostatics. Supporting this statement, the authors failed to detect DNA binding to *Kp*FeoC (Hung et al. 2012a). Furthermore, the authors also observed Zn^{2+} binding (but surprisingly not Fe^{2+} binding) in the winged region of *Kp*FeoC, although this failed to promote DNA binding (Hung et al. 2012a). While *Kp*FeoC did not bind Fe^{2+}, the presence of four conserved Cys residues in the wing region (including a CXXC motif) suggested the possibility of iron-sulfur cluster binding (Fig. 12.9). As such, cellular and biochemical studies have sought to understand the identity and the role of iron-sulfur cluster binding to FeoC.

The determination of the exact nature of the FeoC [Fe-S] cluster was difficult due to its redox- and oxygen-sensitivity. The first biochemical study to investigate the ability of *Kp*FeoC to bind an [Fe-S] cluster was published in 2013. The presence of a paramagnetic center in *Kp*FeoC was first indicated by strong paramagnetic shifts in ^{1}H NMR experiments. Further biophysical characterization of reconstituted *Kp*FeoC (exhibiting only 10% incorporation) under oxic conditions using electronic absorption spectroscopy suggested that the identity of the cluster was either that of a [2Fe-2S] cluster or a [4Fe-4S] cluster (Hsueh et al. 2013). When reconstituted *Kp*FeoC was analyzed by electron paramagnetic resonance (EPR) spectroscopy, experimental *g* values were attributed to the presence of an unusual *hi*gh-*p*otential *i*ron sulfur *p*rotein (HiPIP) cluster (Hsueh et al. 2013). Lastly, X-ray absorption spectroscopy (XAS) confirmed the cluster in *Kp*FeoC to be ligated by four cysteine residues (Hsueh et al. 2013). The role of the cysteine residues in *Kp*FeoC were

evaluated by testing the ability of cysteine to serine variants to bind an iron-sulfur cluster. Three of four of the cysteine residues (Cys^{56}, Cys^{64}, and Cys^{71}) were essential for cluster binding whereas Cys^{61} was not essential (Hsueh et al. 2013). Very surprisingly, the [4Fe-4S] cluster present in *Kp*FeoC had an unusually long average half-life of 17 h upon exposure to oxygen (Hsueh et al. 2013).

The most recent publication that characterized the iron-sulfur cluster in the FeoC protein was published in 2019. In this study, the cluster was reconstituted under strictly anoxic conditions and subsequently characterized by electronic absorption spectroscopy, EPR, XAS, and dynamic light scattering (DLS) (Smith et al. 2019). Reconstituted under anoxic conditions, the cluster of *Ec*FeoC was assigned to the more common redox active $[4Fe\text{-}4S]^{2+/+}$ species (Smith et al. 2019). Electronic absorption spectra of the cluster-bound *Ec*FeoC revealed that the $[4Fe\text{-}4S]^{2+}$ cluster is O_2-sensitive and rapidly degrades to a $[2Fe\text{-}2S]^{2+}$ cluster in ≈5 min ($k_{obs} \approx 0.04\ s^{-1}$) in O_2-replete conditions (Smith et al. 2019). When these experiments were repeated for *Kp*FeoC, nearly identical electronic absorption features, XAS spectra, and EPR signals were observed confirming that *Kp*FeoC also binds a redox active, O_2-sensitive $[4Fe\text{-}4S]^{2+/+}$ cluster (Smith et al. 2019). Lastly, anoxic DLS measurements demonstrated that cluster binding to both *Ec*FeoC and *Kp*FeoC resulted in a compaction of the protein conformation, but cluster binding did not promote oligomerization. Though the exact role of FeoC remains unknown, these data support that FeoC may function as a redox-active iron sensor, similar to that of FNR (Smith et al. 2019). However, some bacteria, such as *V. cholerae* lack the necessary Cys residues that are required to bind an [Fe-S] cluster. Whether these proteins function similarly to cluster-binding FeoCs has yet to be determined.

12.3.5.7 FeoA/B/C Interaction Studies

Despite in vitro studies of small soluble proteins of the Feo system (FeoA and FeoC) and single isolated domains (NFeoB), few studies have investigated how FeoA, FeoB, and/or FeoC may function in concert to transport Fe^{2+} iron across a bacterial membrane. In 2012, the ability of FeoA and FeoB to interact was explored in *Salmonella enterica* using a bacterial two hybrid (BACTH) assay. When *feoB* was deleted from strain JH380 (Δ*mntH,* Δ*sitABCD* background), Fe^{2+} uptake was threefold lower than in the WT, and these results were recapitulated with an *feoA* deletion. Reintroduction of *feoA* was able to rescue the phenotype. In other words, the loss of *feoA* was as detrimental to ferrous iron uptake in *S. enterica* as the loss of *feoB* (Kim et al. 2012). An *feoAB* deletion strain was then created to test whether FeoA function would be dependent on FeoB. Complementation with only *feoB* resulted in Fe^{2+} uptake approximately three-fold lower than JH380, whereas complementation with only *feoA* resulted in no rescue of Fe^{2+} uptake; complementation of both *feoA* and *feoB* restored Fe^{2+} uptake. These results suggest that FeoA is necessary for FeoB to transport ferrous iron in vivo (Kim et al. 2012).

As FeoA-based dependence might be the result of protein-protein interactions between FeoA and FeoB, this hypothesis was further probed in vivo. A BACTH

assay in *S. enterica* where FeoA was fused to T18 and FeoB was fused to T25 was initially constructed, and β-galactosidase activity indicated an interaction between FeoA and FeoB in vivo (Kim et al. 2012). FeoA variants (P20A/L26Q and W9G/L26Q) demonstrated ≈28-fold lower β-galactosidase activity compared to the WT. Single variant studies suggested that L26 may be an essential residue for FeoA-FeoB interactions (Kim et al. 2012). These cellular results support the hypothesis that FeoA is important for FeoB-mediated ferrous iron transport in *S. enterica* (Kim et al. 2012), but the exact mechanism is unknown.

The presence of the FeoC HTH motif suggests that the protein could serve as a transcriptional regulator of the Feo system, which could be linked to the protein's cluster composition. As such, studies have examined how FeoC affects the expression levels of the *feoB* gene in *S. enterica* (Kim et al. 2013). Maximal expression of *feoB* occurs under both low iron and low O_2 conditions, which could be further enhanced in the absence of a functional *fur* gene or impaired in the absence of a functional *fnr* gene (Kim et al. 2013). A *feoC* deletion strain exhibited low levels of *feoB* expression, which could be restored by complementation with an *feoC*-containing plasmid. Interestingly, levels of *feoB* mRNA were higher in this strain than in the WT suggesting that *feoC* does not act at the point of transcription, but rather post-transcriptionally (Kim et al. 2013). BACTH experiments demonstrated that FeoB and FeoC interact, and these results were confirmed using pulldown experiments with NFeoB and His_6-FeoC, although the oxidation state and metal-bound form of FeoC was not controlled. *S. enterica* harboring both a *feoC* and a *ftsH* deletion resulted in lower levels of FeoB suggesting that FeoC may protect FeoB from proteolysis by FtsH. Additionally, a Δ*feoC* strain of *S. enterica* accumulated 4.5-fold less Fe^{2+} than the WT strain indicating that the FeoC protein is important for Fe^{2+} uptake in vivo (Kim et al. 2013). A follow-up study investigated Lon-mediated proteolysis of FeoC in *S. enterica* (Kim et al. 2015). FeoC expression from an IPTG-inducible plasmid in *S. enterica* was only detectable under low-oxygen conditions and did not appear to be affected by low- or high-iron concentrations. Interestingly, the FeoC protein was rapidly degraded when expressed in cells growing in a high-oxygen and high-iron environment ($t_{½}$ ca. 5 min), similar to the rate of the O_2-mediated cluster decomposition. A switch to anoxic conditions increased FeoC stability ($t_{½}$ ca. 50 min) and was unaffected by the presence of absence of iron (Kim et al. 2015). Mutation of all four Cys residues in the wing of FeoC, the likely sites for binding of an iron-sulfur cluster as shown in *K. pneumoniae* and *E. coli*, further increased FeoC stability. Additionally, FeoC stability appears to affect the accumulation of FeoB. In the absence of the Lon-protease, FeoC can accumulate under both high- and low-oxygen conditions which promotes the accumulation of FeoB (Kim et al. 2015). The authors suggest that this could be a method by which *S. enterica* regulates Feo-mediated Fe^{2+} uptake under anoxic and iron-limiting conditions, when regulation but FUR and FNR would be negligible (Kim et al. 2015). Binding of an iron-sulfur cluster to FeoC could serve to control the oxygen-sensitivity of FeoC; however, no studies have examined how cluster binding affects FeoC stability and degradation.

In *Vibrio cholera*, the causative agent of the disease cholera, the Feo system is composed of FeoA, FeoB, and FeoC, which may interact to regulate Feo-mediated Fe^{2+} transport (Weaver et al. 2013). A BACTH assay was performed to assess interactions between and among the Feo proteins. No interactions were detected between FeoA-FeoB or FeoA-FeoC. In contrast, this method did reveal an interaction between FeoB and FeoC, which was mapped to the N-terminal domain of FeoB. E29G and M35A variants of FeoC abolished the FeoB-FeoC interaction, but conservation of these residues is poor among γ-proteobacteria (Weaver et al. 2013). In contrast to these first studies, later work on the *V. cholerae* Feo system suggested that FeoA, FeoB, and FeoC all interact to form a large complex. In 2016, in vivo formaldehyde cross-linking was used to probe which Feo complexes might be present or active in vivo. Several higher-order complexes of FeoA, FeoB, and FeoC were observed localized to the inner membrane based on SDS- and blue native-PAGE. The complexes were estimated to be ≈250 kDa, ≈500 kDa, and ≈720 kDa. Immunoprecipitation and LC-MS/MS demonstrated that FeoA and FeoB could be detected in the complex at ≈720 kDa, but not FeoC. However, when the V5 tag for immunoprecipitation was placed on FeoC instead of FeoB, then FeoC could be detected in the largest complex suggesting that the tag may hinder FeoB-FeoC interaction (Stevenson et al. 2016). The exact stoichiometry of the large complex (≈720 kDa) could not be determined, but it was suggested that a trimer of FeoB trimers may interact with one or more FeoA or FeoC proteins to transport ferrous iron (Stevenson et al. 2016). Some additional complexes were found to contain only FeoB, while a complex at ≈100 kDa was found to contain FeoA, FeoB, and FeoC. Smaller complexes were proposed to be intermediates or possibly products from the disassembly and the breakdown of a larger Feo complex. Additionally, when FeoA was tagged with the V5 epitope for immunoprecipitation, the protein could not be detected in any complexes (Stevenson et al. 2016). It could not be determined which, if any, of these complexes are dominant within the cell, but these results do suggest that all three of the Feo proteins may interact at some point within the cellular context.

Mutational analyses have given some insight into how a larger Feo complex may form in *V. cholerae*. For example, an FeoB K15D variant in the G1 motif abolished Feo function and resulted in no detectable complex formation, indicating that nucleotide binding may be important for protein-protein interactions. An FeoB variant of the switch II region, D72A, resulted in the loss of function and the inability to form a larger complex (Stevenson et al. 2016). In an FeoC deletion strain, FeoB was found expressed at lower levels in the inner membrane, yet an FeoA-FeoB complex was still observed, suggesting that FeoC plays a role in FeoB expression but is not required for complex formation. In contrast, plasmid-driven expression of FeoB in tandem with any of four FeoA variants (G32K, A45D, P50R, and V72K) failed to display complex formation, suggesting that intact FeoA is a pre-requisite for Feo interactions (Stevenson et al. 2016). Further structural studies on Feo protein complexes would be useful in clarifying why and how these variants lead to disruption in complex formation.

Finally, structural and biophysical measurements have shown an interaction between *Klebsiella pneumoniae* NFeoB and its cognate FeoC. ITC experiments of nucleotide-free *Kp*NFeoB and apo *Kp*FeoC titrations demonstrated a 1:1 molar interaction with a K_d of ≈0.5 μM, and SEC experiments revealed co-migration of monomeric, nucleotide-free *Kp*NFeoB with apo, monomeric *Kp*FeoC (Hung et al. 2012b). These observations were supported by an X-ray crystal structure of nucleotide-free *Kp*NFeoB co-crystallized with apo *Kp*FeoC. Each asymmetric unit contained one nucleotide-free *Kp*NFeoB and one apo *Kp*FeoC in which the N-terminus of FeoC interacted with the GDI domain of NFeoB (Hung et al. 2012b). Unfortunately, the wing region of FeoC was not present in electron density, likely a result of the flexibility of the wing region (Hung et al. 2012b). Additionally, this dynamic region of *Kp*FeoC is known to interact with an [Fe-S] cluster, which was not probed. Thus, it is unclear whether either [Fe-S] cluster binding or possibly nucleotide binding would affect this NFeoB-FeoC interaction and how.

12.4 Metal-Rich, Anoxic, and Acidic Environments

Iron-oxidizing bacteria (FeOB) utilize the oxidation of Fe^{2+} to Fe^{3+} as a means to generate energy for growth. These organisms obtain the iron necessary for essential metabolic processes from their native environment and play an important role in the iron biogeochemical cycle (Emerson et al. 2010). Given the insolubility of Fe^{3+}, and the production of ROS upon spurious Fe^{2+} oxidation, iron-dependent survival presents a unique challenge to FeOB. Furthermore, the energy derived from abiotic Fe^{2+} oxidation is low (≈29 kJ mol^{-1}) near neutral pH, and the half-life of Fe^{2+} under oxic conditions is <1 min (Emerson et al. 2010; Roden et al. 2004). FeOB living under these conditions would therefore produce iron oxyhydroxides, which would be detrimental to the organism. As a result, FeOB must grow under microaerophilic conditions that stabilize Fe^{2+} over Fe^{3+} (Emerson et al. 2010; Roden et al. 2004). FeOB inhabit a variety of ecological niches including the soil, freshwater and marine environments, waste and bioreactor sites, and hydrothermal vents (Emerson et al. 2010). A greater understanding how FeOB transport Fe^{2+} would thus improve our understanding of their contribution to the iron biogeochemical cycle and would shed light on this ancient form of metabolism.

In contrast to FeOB, iron-reducing bacteria (FeRB or IRB) generate energy by reducing Fe^{3+}, typically from insoluble iron oxides, to Fe^{2+}. Bacteria that couple this process to the oxidation of organic molecules, such as sugars and amino acids, aromatic compounds, long chain fatty acids, and butyrate, propionate, and acetate or H_2 are termed dissimilatory iron reducing bacteria (Esther et al. 2015; Lovley 1997; Richter et al. 2012; Weber et al. 2006). These organisms can often be found cohabitating with FeOB because the Fe^{3+} produced may function as an FeRB feedstock. FeRB play a role in mineral formation, such as when reduced iron is exposed to oxygen, and iron cycling (Lovley 1997; Esther et al. 2015; Richter et al. 2012; Weber et al. 2006). Reduction of Fe^{3+}-rich surfaces can be accomplished via

several routes. One of these routes is by direct contact of a bacterial biofilm with an Fe^{3+}-rich surface, as the biofilm may help mediate electron transfer. Fe^{3+} reduction can also be facilitated by chelators or siderophores that solubilize Fe^{3+} and increase its bioavailability (Esther et al. 2015; Lovley 1997; Thormann et al. 2004; Richter et al. 2012; Weber et al. 2006). Additionally, FeRB can cycle electron shuttles to reduce Fe^{3+}-rich surfaces. Somewhat similar to biofilm contact, pili, or protein nanowires, can also mediate contact with Fe^{3+}-rich surfaces for reduction (Esther et al. 2015; Richter et al. 2012; Brutinel and Gralnick 2012; Weber et al. 2006). Unfortunately, the iron transport mechanisms in these bacteria remain largely uncharacterized, but a synopsis of what is currently known in the literature is presented below.

12.4.1 Magnetotactic Bacteria

Magnetotactic bacteria (MB), microorganisms that orient themselves and move along Earth's magnetic field through a process known as magnetotaxis, were first discovered in 1975 (Blakemore 1975). MB were isolated from samples taken from surface sediments of salt marshes and surface layers of sedimentary cores in Massachusetts (Blakemore 1975). Using transmission electron microscopy (TEM), crystal-like particles that are now termed magnetosomes were initially discovered. At that time, it was posited that these intracellular compartments might be magnetic, formed from a mineral such as magnetite. Supporting this presumption, energy dispersive X-ray microanalysis subsequently revealed these particles to be composed predominantly of iron. Concurrently, different species of morphologically distinct MB were also identified in several other marsh muds (Blakemore 1975). In 1988, MB isolated from an estuarine salt marsh were analyzed for elemental content of the magnetic particles, which were determined to be composed of iron and oxygen in the form of magnetite (Fe_3O_4) constituting ca. 1.6% of the dry weight of the organism (Bazylinski et al. 1988). Variations in particle composition, comprising iron and sulfur in the form of greigite (Fe_3S_4) and pyrite (FeS_2), were then found (Mann et al. 1990) and can be correlated to distinct growth environments.

MB are diverse microorganisms that grow optimally within anoxic and microaerophilic environments, but they can also be isolated from deep sea sediments. In the deep oceans, MB are proposed to play an important role in marine iron and sulfur cycling as accumulated, intracellular iron and sulfur can be released into the environment upon cell death and lysis thus promoting additional microbial activity (Simmons et al. 2004). High concentrations of particulate iron support a high abundance of MB, and this environment occurs at the oxycline, the point in the aquatic environment where the concentration of oxygen changes steeply and beyond which sulfur concentrations begin to peak (Simmons et al. 2004). MB appear to be widely distributed among the bacterial kingdom, including the classes α- through ε-proteobacteria, *Chlorobiales*, and Cyanobacteria, among others (Simmons et al. 2004). Due to their high iron requirements and their anoxic and microaerophilic

growth environments, it is likely that the iron acquisition systems present in MB mimic those present on early Earth, providing a glimpse of life prior to the GOE.

Consistent with their high demand for iron, MB must utilize a combination of tactics to accumulate this essential element. One major strategy is the use of siderophores. Like MB, many (but not all) prokaryotes engage in the metabolically-demanding biosynthesis and secretion of siderophores to scavenge for ferric iron. Retrieved ferric iron trapped in these siderophores can be released by either destruction of the siderophore itself via bond cleavage, or through a ferric reductase-mediated iron reduction and release mechanism (Cain and Smith 2021). Importantly, as MB are found in a number of anoxic niches, ferrous iron acquisition also represents a major acquisition route of reduced environmental iron.

Magnetospirillum magneticum strain AMB-1 relies on catechol and hydroxamate siderophores as well as ferrous iron transport as its primary means of iron uptake (Calugay et al. 2003). A global expression analysis of the *M. magneticum* strain AMB-1 genome has revealed multiple iron-regulated genes in this organism. In magnetosome-forming cultures, approximately 70% of extracellular iron was rapidly assimilated within 1 h (Suzuki et al. 2006). Under these conditions Fe^{2+} transport genes (*ftr1*, *tpd*, *feoA*, and *feoB*) were upregulated whereas in non-magnetosome-forming conditions ferric iron uptake genes (such as *tonB*, *fepA*, and *napABC*) were down-regulated (Suzuki et al. 2006). In contrast to the down-regulated ferric iron uptake genes, *cirA* and *fepC* were upregulated in iron-replete conditions and encode a ferric-siderophore outer membrane receptor and an inner membrane ferric-siderophore transporter, respectively (Suzuki et al. 2006). *M. magneticum* strain AMB-1 is capable of growing under oxic conditions (Matsunaga et al. 1991), and at least one catechol siderophore has been identified to be 3,4-dihydroxybenzoic acid (Calugay et al. 2006). Siderophore-mediated ferric iron uptake was significant when concentrations of ferric iron in the medium were 40–80 μM (Calugay et al. 2003), but this condition is not conducive to magnetosome formation.

When taken together, these results indicate that Fe^{2+} uptake is likely the predominant source of iron under magnetosome-forming conditions (Suzuki et al. 2006), and there seems to be more than one route for ferrous iron assimilation. Ftr1 is uncharacterized but annotated as a Fe^{2+}/Pb^{2+} permease, Tpd is uncharacterized but annotated to be involved in high-affinity Fe^{2+} uptake, and Amb3335 is predicted to be a ferric iron reductase, which is also upregulated in iron-replete conditions (Suzuki et al. 2006). In a nonmagnetic mutant of *M. magneticum* strain AMB-1 deficient for siderophore uptake (denoted strain NMA61), a cytoplasmic ATPase that contributes to Fe^{2+} uptake was also identified (Suzuki et al. 2007). This ATPase bears homology to ArgK, a protein kinase (Suzuki et al. 2007). Previous reports speculate that the ATPase may provide energy for a Fe^{2+} transporter such as Feo, Tpd, and Frt1, thus supplying ferrous iron to magnetosome formation (Suzuki et al. 2007). In 2008, iron transporters expressed in *M. magneticum* strain MS-1 were identified using 2-D electrophoresis by comparing proteins expressed during growth in Fe^{2+}- and Fe^{3+}-rich media (Taoka et al. 2009). Two of the proteins expressed under Fe^{2+}-rich conditions were 76 kDa and 70 kDa in size and with homology to TonB-dependent outer membrane ferric-siderophore receptors in *Beijerinckia indica*

and *Rhodopseudomonas palustris*, respectively (Taoka et al. 2009). Two sets of the *feoA* and *feoB* genes were also identified in this study. Expression of FeoB was confirmed by utilizing polyclonal antibodies generated from recombinant NFeoB1. In these studies, FeoB appears as a band at ≈75 kDa localized to the cytoplasmic membrane, consistent with predictions of FeoB's location (Taoka et al. 2009). Further functional studies have yet to be reported.

M. gryphiswaldense MSR-1 does not secrete siderophores but does utilize Fe^{3+} through extensive ferric reductase activity and subsequent Fe^{2+} uptake. Ferric reductase activity in whole cells, the cytoplasm, and membrane fractions (but not the periplasm) of *M. gryphiswaldense* was first demonstrated in 2007 (Xia et al. 2007). Native PAGE coupled with ferric reductase active staining afforded the identification of six bands in the cytoplasmic fraction and three bands in the membrane fraction of cells corresponding to ferric reductase isozymes. These ferric reductases were named FeR-1 to FeR-6. FeR-6 was subsequently purified as it had the greatest activity among all of the reductases. FeR-6 is ≈16 kDa and does not appear to have sequence homology to other proteins (Xia et al. 2007). Ferric citrate, reduced nicotinamide adenine dinucleotide (NADH), and oxidized flavin mononucleotide (FMN) were used in ferric reductase assays to determine the reductase activity of FeR-6. The protein had a modest K_M for ferric citrate of ≈45 μM and a V_{max} of ≈1.2 μM/min. Interestingly, ferric reductase activity was strongly inhibited by Ag^+ and divalent metal ions such as Zn^{2+}, Mn^{2+}, Cu^{2+}, and Co^{2+} (Xia et al. 2007). In a follow-up study, FeR-5 and FeR-6 were identified as bifunctional enzymes with thioredoxin reductase activity and flavin reductase activity, respectively, and deletion of both genes inhibited magnetosome formation (Zhang et al. 2013). Although FeR-6 could reduce Fe^{3+} without the FMN cofactor, Fe^{3+} reductase activity was 20-fold higher with FMN (Zhang et al. 2013), emphasizing the importance of the flavin cofactor. The remaining four isozymes have not yet been characterized.

As the ferric reductases are located in the cell membrane, they are speculated to provide reduced iron for transport via a membrane Fe^{2+} transporter (Zhang et al. 2013). Early studies examining the growth and magnetosome formation of *M. gryphiswaldense* MSR-1 indicate that magnetite formation can only occur under microaerophilic conditions and is tightly coupled to iron uptake (Schüler and Baeuerlein 1998). Under these conditions, recent experiments suggest that ferric reductase activity could supply the inner membrane transporter FeoB with Fe^{2+}, which is then transported into the cell for magnetosome incorporation. In 2008, two *feoB* genes in *M. gryphiswaldense* strain MSR-1 were identified and characterized (Rong et al. 2008). The predicted FeoB1 protein encoded by the *feoB1* gene (704 amino acids) has high sequence identity to FeoBs from other magnetotactic bacteria but only 35% identity (53% similarity) to FeoB2, encoded by *feoB2*. A putative *feoA* gene was found within the region of *feoB1* and named *feoA1*. FeoB1 contains conserved G-protein motifs in the N-terminal region, and the C-terminal domain was predicted to be imbedded in the cytoplasmic membrane by 9 TM helices (Rong et al. 2008). TEM was used to monitor magnetosome formation of a Δ*feoB1* strain, which produced lower amounts of magnetosomes, smaller magnetosomes, and lower iron content compared to the WT strain. These defects could be rescued by

complementation with *feoB1*. Similar results were observed for cells grown in the presence of either Fe^{2+}- or Fe^{3+}-citrate (Rong et al. 2008). The *feoA1* and *feoB1* genes were also found to be downregulated under iron-rich conditions. A later study investigated the role of *feoB2* in *M. gryphiswaldense* MSR-1 (Rong et al. 2012). Interestingly, when a Δ*feoB2* strain was analyzed for magnetosome formation, the size and number of the magnetosomes were similar to the WT strain suggesting that FeoB2 does not contribute to magnetosome formation when FeoB1 is present. Surprisingly, in cells lacking both a functional FeoB1 and FeoB2, magnetosome formation and size was similar to that of WT; however, the number of magnetosomes per cell were lower in the double mutant than in the *feoB1* deletion strain. Additionally, when cells were grown in the presence of ferric citrate, the Δ*feoB2* strain had significantly lower levels of cellular iron content than that of the Δ*feoB1* strain (Rong et al. 2012). For all deletion strains, the cellular metal content of Mn, Zn, Cu, and Mg was similar to WT confirming that both FeoBs are dedicated to iron uptake (Rong et al. 2012). The deletion strains were also tested for their ability to respond to oxidative stress. Deletion strains demonstrated sensitivity when grown in 500 μM H_2O_2, and all had significantly lower superoxide dismutase and catalase activities when compared to the WT strain (Rong et al. 2012), suggesting that some of the acquired ferrous iron is necessary for assimilation into these two essential enzymes that combat oxidative stress.

12.4.2 Gallionella *and* Geobacter

Gallionella ferruginea, a microaerophilic bacterium with a growth requirement for Fe^{2+}, was first described in 1837 and is the first known FeOB to be identified. *G. ferruginea* has an intriguing ability to form an Fe-oxyhydroxide-encrusted stalk during growth (Emerson et al. 2010). *G. ferruginea* is able to grow at the end of the stalk, which can form at a rate of 80–90 μm/h in microcultures. These stalks are likely used as a positioning mechanism to find the appropriate iron/oxygen gradients needed for *G. ferruginea* growth, but they may also function as a sink to deposit precipitated iron oxyhydroxides that would otherwise result in the death of the organism (Hanert 1974; Emerson et al. 2010). Questions remain regarding the composition of the stalks and the mechanism by which the precipitated iron is excreted.

While Fe^{2+} transport mechanisms have not been well-characterized in *Gallionella*, this transport process undoubtedly contributes to the ability of this organism to cycle iron in different and often harsh iron-rich environments. Acid mine drainage (AMD) sites are low-pH, anoxic springs containing high levels of iron as a result of mining (Jones et al. 2015). The Upper and Lower Red Eyes in Pennsylvania constitute an AMD with pH ranging from 4.0–4.5 and Fe^{2+} concentrations >6.5 mM. FeOB, such as *Gallionella*, offer the possibility to bioremediate such sites using biological iron oxidation (Jones et al. 2015). An analysis of free-living bacteria at this site showed that the *Gallionellaceae* family composed 42% of

all bacterial species identified. Bacteria from the orders of *Rhodospirillales*, *Acidimicrobiales*, *Xanthomonadales*, *Acidobacteriales*, and *Nitrospira* were also present, but their distribution was dependent on both pH and [Fe^{2+}]. For instance, *Gallionellaceae* were more abundant at high Fe^{2+} concentrations while *Acidithiobacillus* spp. were more abundant at lower Fe^{2+} concentrations (Jones et al. 2015). Though not as well characterized, the Arctic tundra also contains regions where FeOB inhabit acidic soils, sediment surfaces, and water sources. *Gallionella* spp. have been identified in all of these environments (Emerson et al. 2015). Thus, it is clear that adaptation to high acidic environments that may be rich in Fe^{2+} is necessary to support the survival of *Gallionella* and related species.

Similarly adapted is *Geobacter sulfurreducens*, a hydrogen- and acetate-oxidizing, dissimilatory metal- and sulfur-reducing bacterium that can be found in soils, aquatic sediments, and subsurface environments. Reduction of insoluble minerals such as Fe^{3+} oxides is facilitated by electron transport through pili rich in *c*-type cytochromes, which are localized to the periplasm and often excreted into the extracellular space (Caccavo et al. 1994; Lovley and Walker 2019; Weber et al. 2006; Smith et al. 2013; Seeliger et al. 1998). Though iron transport has not been extensively studied in *Geobacter*, one study analyzed the *Geobacter* iron stimulon by determining differences in gene expression for cells growing in iron-replete, iron-sufficient, and iron-deficient conditions. Genes differentially expressed in *Geobacter* encoded for *c*-type cytochromes and other proteins containing heme or iron-sulfur clusters, and Fe^{3+} reductases such as the OmcZ cytochrome (Embree et al. 2014). Both FeoA and FeoB were the most downregulated during Fe^{3+} reduction, suggesting that Fe^{2+} generated from reduction is not used as a substrate for the Feo system. Eleven efflux pumps/subunits and one ferritin-like protein domain were also downregulated, while another ferritin-like protein domain was upregulated (Embree et al. 2014). The Fur and IdeR proteins were more highly expressed under iron-sufficient conditions and exhibited repression as extracellular Fe^{2+} concentrations increased. These results suggest that iron homeostasis is tightly regulated in *Geobacter* in response to the large amounts of Fe^{2+} produced from metabolic processes and to maintain intracellular iron stores (Embree et al. 2014). Future characterization of *Gallionella* and *Geobacter* could lead to the ability to tailor these metal-tolerant bacteria for bioremediation purposes.

12.4.3 Shewanella

Shewenella oneidensis MSR-1 is both a facultative anaerobe and a dissimilatory metal-reducing bacterium that inhabits aquatic environments and iron rich-sediments, and can use oxidized iron as a terminal electron acceptor (Bennett et al. 2015). As respiration occurs, Feo-transported Fe^{2+} accumulates inside of the bacterium and becomes incorporated into iron-utilizing proteins and solid-phase minerals (Bennett et al. 2015). In addition to Feo, *Shewanella* may possess another uncommon Fe^{2+} import system. The MgtE protein is a Mg^{2+}/Co^{2+} transporter first

identified in *Bacillus firmus* (Smith et al. 1995) but present in *S. oneidensis* MR-1, which contains three *mgtE* homologs. One of these homologs (*SO_3966*) is found in 26 of 36 *Shewanella* genomes and has been named the *f*errous *i*ron and *c*obalt *i*mporter (FicI) (Bennett et al. 2018). A role in Fe^{2+} uptake was proposed upon observations that a Δ*ficI* strain of *Shewanella* conferred resistance to Fe^{2+}. This hypothesis was confirmed by measuring Fe^{2+} uptake in a Δ*ficI* strain which was ≈90% lower than that of the WT strain and also displayed Co^{2+} and Mg^{2+} sensitivity (Bennett et al. 2018). However, it seems that the FicI system is less important than the Feo system when iron is scarce, as the Δ*feoB* strain was unable to grow under iron-limiting conditions unlike the Δ*ficI* strain. It is suggested that FeoB serves as the primary Fe^{2+} transporter for *Shewanella* while FicI serves as a secondary Fe^{2+} transporter.

Due to its high rate of Fe^{2+} acquisition, *Shewenella* has had to adapt mechanisms to prevent iron overload (Bennett et al. 2015; Carlson et al. 2012; Dunning et al. 1998). One such mechanism is through the use of a ferrous iron exporter encoded by the gene locus *SO_4475* and named FeoE (herein referred to as *So*FeoE), although it is not associated with the *feo* operon. FeoE is predicted to be a member of the cation diffusion facilitator (CDF) family, which is a family of inner membrane proteins that efflux divalent metal ions using the proton motive force (Bennett et al. 2015; Nies and Silver 1995; Paulsen and Saier 1997). *So*FeoE shares sequence similarity and identity (≈60% and ≈48%, respectively) with the YiiP (FieF) protein from *E. coli*, which has been shown to export Zn^{2+}, Cd^{2+} and Fe^{2+} (Chao and Fu 2004; Wei and Fu 2005; Grass et al. 2005b). *So*FeoE was also previously shown to export Zn^{2+} and Cd^{2+}, but had not been tested for its ability to export Fe^{2+}, either in vitro or in vivo (Coudray et al. 2013). One study examined the ability of *So*FeoE to protect *S. oneidensis* MSR-1 against Fe^{2+} toxicity when utilizing ferric citrate for anaerobic respiration by examining the survivability of Δ*feoE* strains. *S. oneidensis* deficient for *feoE* exhibited a growth defect compared to the WT strain but could be rescued with complementation by *feoE* (Bennett et al. 2015). Ferrozine assays measuring Fe^{2+} directly resulting from ferric citrate respiration were similar for both deletion and WT strains, supporting the hypothesis that respiration on ferric citrate is not impaired in the Δ*feoE* strain, but functions to prevent Fe^{2+} toxicity (Bennett et al. 2015). This assertion was further supported by lower growth rates of the Δ*feoE* strain when grown in the presence of 1 mM $FeCl_2$, and by iron retention assays demonstrating that *feoE* deficient *S. oneidensis* retain significantly more iron than the WT *S. oneidensis* (Bennett et al. 2015). Sensitivity of the Δ*feoE* strain was tested against a range of divalent metal ions and *feoE* was found to be specific for Fe^{2+}, in contrast with the previous suggestion of metal promiscuity (Bennett et al. 2015). Furthermore, the FeoE protein is conserved amongst *Shewanella* spp. suggesting that it is a common mechanism to protect against Fe^{2+} toxicity. Homologs of FeoE may also be present in *Geobacter metallireducens* and *Geobacter sulfurreducens*, but share a much lower sequence similarity (Bennett et al. 2015).

Ferrous iron uptake likely accounts for one of the dominant iron sources in this bacterial family, as *Shewanella* encode for just one natural siderophore, putrebactin (Pub), synthesized by the *pubABC* operon using putrescine as a precursor. The

TonB-specific ferric siderophore receptor is encoded by *putA* and the Pub reductase is encoded by *putB* (Ledyard and Butler 1997; Kadi et al. 2008; Soe and Codd 2014; Liu et al. 2018). A spontaneous mutant of *S. oneidensis*, SO-X2, was identified and believed to be deficient for cytochrome *c* production as colonies of *S. oneidensis* appeared white instead of red (Dong et al. 2017). However, this was not the result of a mutation within the cytochrome *c* biosynthesis genes, but rather due to a mutation in the *putA* gene (Dong et al. 2017). The deletion of *putA* resulted in an ≈50% decrease in intracellular iron concentration when compared to the WT and also resulted in colorless colonies as the inability of the Δ*putA* strain to deliver iron to the cytosol has downstream effects on *Shewanella's* ability to produce both cytochrome *c* and heme (Dong et al. 2017; Liu et al. 2018). Correlating with these results was the observation that the Δ*putA* strain also produced Pub at a significantly higher level under iron-limiting conditions compared to the WT (Dong et al. 2017). Knockouts of the *pub* operon and *putB* were also tested for their effects on iron uptake in *Shewanella*. Both Δ*pub* and Δ*putB* strains exhibited normal levels of intracellular iron, though the Δ*pub* strain was incapable of producing Pub. This result indicates the presence of a primary functional iron uptake system, such as Feo, that is capable to circumventing this loss (Liu et al. 2018). In this study, a Δ*feo* deletion strain had a lower total iron concentration than the WT, but also had significantly more total iron than the Δ*putA* strain. However, loss of *feo* appeared to be more detrimental to *Shewanella* growth when compared to the growth of the Δ*putA* strain. A double deletion strain grew poorly under iron depleted conditions, but could grow at Fe^{2+} concentrations of 0.5 mM and higher, likely using FicI as a secondary Fe^{2+} transporter (Liu et al. 2018). Thus, it is clear that ferrous iron uptake contributes strongly to iron homeostasis in *Shewanella*, and it is likely that similar mechanisms may be operative in other FeOB and FeRB, although more characterization is warranted.

12.5 The Host-Pathogen Interface

Among other functions, humans depend on mononuclear and dinuclear iron proteins for carnitine biosynthesis, hypoxic sensing, DNA biosynthesis, and functionalization of unsaturated lipids. Additionally, cellular iron is also incorporated into [Fe-S] clusters and utilized in heme biosynthesis, both of which serve as cofactors for enzymes involved in gene regulation, oxygen transport, and even drug metabolism (Hider and Kong 2013; Ganz 2008). The labile iron pool is composed mostly (>80%) of Fe^{2+}, with iron concentrations estimated to be between ca. 10^{-7} M and ca. 10^{-6} M in either erythroid cells or hepatocytes (Hider and Kong 2013). By way of comparison, one estimate places free iron concentrations in human serum at $\approx 10^{-24}$ M (Fischbach et al. 2006). Because ferrous iron is significantly more soluble and more kinetically labile compared to ferric iron at physiological pH (≈7.4), ferrous iron is typically the species that is transported into cells, translocated within cells, and even incorporated into iron-dependent enzymes and proteins (Hider and Kong 2013). Thus, the prevalence of Fe^{2+} in human enzymes

and within the labile iron pool suggests that invading microbes might encounter a significant amount of Fe^{2+} within their colonization niches.

The concentration of iron in the labile Fe^{2+} pool is governed by several factors. The amount of iron required for normal physiology may differ among both organisms and cells (e.g., mitochondria have a higher iron requirement since that is where heme and iron-sulfur cluster biosyntheses take place). One mechanism for regulating the intracellular labile iron pool is to control the rate of iron transport into cells by divalent metal ion transporters (Hider and Kong 2013). Iron within the labile iron pool can be temporarily depleted be oxidation of iron and storage within ferritins. Finally, iron efflux via ferroportin can also control the concentration of the labile iron pool, preventing iron overload and potential redox stress within the cell (Hider and Kong 2013). Together, these mechanisms maintain iron homeostasis in humans, and these systems are tightly regulated to control iron availability during times of infection.

Iron homeostasis in humans and animals is heavily altered during microbial infection. One of the host's first defense mechanisms against invading pathogens is to reduce the absorption of dietary iron. The host also sequesters iron already present in the extracellular space to further limit the availability of this essential nutrient to pathogens. These processes combined are often termed "iron withholding" and constitute a part of the host defense mechanism known as nutritional immunity (Ganz 2008; Abu Kwaik and Bumann 2013; Skaar 2010). Bacteria are estimated to require cytoplasmic iron pools at a concentration of $\approx 10^{-6}$ M, and the host can significantly limit the amount of iron available to microbes depending on the niche in which they colonize. In response, bacteria must overcome these limiting conditions in order to survive (Fischbach et al. 2006). Some pathogens have adapted to live within the cytosol of eukaryotic cells where essential nutrients, including iron, are plentiful. Bacteria may also secrete proteases that degrade host proteins and enzymes, releasing essential nutrients that may be acquired by pathogens (Parrow et al. 2013). One important mechanism utilized by bacteria to establish infection is Fe^{2+} uptake driven predominantly by the Feo system. This section summarizes our knowledge of ferrous iron acquisition during infection of unicellular pathogens, which is strongly linked to the Feo system.

12.5.1 Cellular Studies of Ferrous Iron Acquisition at the Host-Pathogen Interface

Helicobacter pylori is the causative agent of chronic gastritis and though several virulence factors had been identified in *H. pylori*, its mechanisms of iron transport and homeostasis are not well understood. *H. pylori* does not appear to produce siderophores but relies on both Fe^{2+} and heme uptake as well as iron sequestered from human lactoferrin. *H. pylori* also possesses ferric reductase activity, which likely facilitates Fe^{2+} transport via the Feo system (Velayudhan et al. 2000).

Inactivation of *feoB* in *H. pylori* significantly reduced the rate of ^{55}Fe uptake regardless of oxidation state, and this phenotype could be restored by complementation with *feoB*. Fe^{2+} uptake kinetics have revealed that FeoB constitutes a high affinity Fe^{2+} transporter (apparent Michaelis constant of ca. 0.5 μM), and the presence of a second, unidentified, low affinity Fe^{2+} transporter was also suggested. Though FeoB is considered to be specific for Fe^{2+} transport, the presence of Cu^{2+} in a 100-fold excess of Fe^{2+} inhibited Fe^{2+} uptake by 74%, while Co^{2+}, Mn^{2+}, Ni^{2+}, and Zn^{2+} had no inhibitory effect on Fe^{2+} transport (Velayudhan et al. 2000). Intriguingly, the ATP synthesis inhibitor, DCCD, strongly inhibited Fe^{2+} transport, perhaps due to NTP promiscuity of this organism's FeoB. Inhibition also occurred in the presence of orthovanadate, a molecule that inhibits ATP hydrolysis. These results suggested that FeoB-mediated Fe^{2+} transport could utilize active ATP hydrolysis as an energy source for the transport process (Velayudhan et al. 2000).

Legionella pneumophila colonizes human macrophages and freshwater amoebae within a parasitic vacuole, where Fe^{2+} likely dominates (Robey and Cianciotto 2002). An *feoB* mutant transported virtually no radiolabeled Fe^{2+} but did not exhibit complete attenuation for extracellular growth in iron-limited media. However, the *feoB* mutant also confers increased resistance to the antibiotic streptonigrin, a direct result of decreased iron pools in the mutant as streptonigrin toxicity is iron-dependent (Robey and Cianciotto 2002). Upon co-culturing the *feoB* mutant with the amoeba *Hartmannella vermiformis* under iron-limiting conditions, the mutant strain was detected at a significantly diminished concentration, indicating that FeoB is necessary for growth and survival in *L. pneumophila* (Robey and Cianciotto 2002). The role of FeoB for intracellular colonization and survival was confirmed in a human macrophage model where the mutant *L. pneumophila* was attenuated in its ability to kill macrophages. Furthermore, a mouse model of infection demonstrated that the lungs of the mice contained lower concentrations of the *feoB* mutant compared to the WT, confirming the importance of *feoB* to *L. pneumophila* virulence (Robey and Cianciotto 2002).

Campylobacter jejuni is a causative agent of foodborne gastroenteritis, and the connection between FeoB and *C. jejuni* pathogenesis was first investigated in 2003 (Raphael and Joens 2003). Iron uptake and growth of different *C. jejuni* strains were compared to that of *E. coli* W3110. The acquisition of $^{55}Fe^{2+}$ in *C. jejuni* was generally lower than that of *E. coli* W3110 (Raphael and Joens 2003). An insertion mutation of *feoB* in *C. jejuni* was then analyzed for $^{55}Fe^{2+}$ uptake and rates were similar to those observed in the WT strains. The experiments were repeated with a *feoB* mutation strain generated through allelic exchange, but no difference in $^{55}Fe^{2+}$ uptake was observed, suggesting $^{55}Fe^{2+}$ uptake was not mediated by FeoB and that FeoB was not be required for Fe^{2+} uptake in *C. jejuni* (Raphael and Joens 2003). However, a later study reinvestigated the role of FeoB in *C. jejuni* as the genomes for the strains previously investigated had not been sequenced, and the presence of an additional FeoB homolog could not be precluded (Naikare et al. 2006). In *C. jejuni* NCTC 11168, *feoA* and *feoB* were found to be cotranscribed and thus constituted an operon. Interestingly, *feoA* expression was elevated six to eight-fold over that of the WT strain in *feoB* mutants (Naikare et al. 2006). Furthermore, the *feoB* mutant

acquired Fe^{2+} at ten-fold less compared to the WT strain. Isolation of spheroplasts from the WT and Δ*feoB* strain showed that 90% of the transported iron was contained within the cytosol, suggesting that *C. jejuni* can also transport Fe^{2+} via a different transporter (Naikare et al. 2006). FeoB also promoted the growth of *C. jejuni* in iron limited media compared to the Δ*feoB* strain. Analysis of iron content during these experiments revealed that a majority of accumulated $^{55}Fe^{2+}$ in the Δ*feoB* strain was localized in the periplasm suggesting the lack of a functional inner membrane transporter (Naikare et al. 2006). *C. jejuni* 81-176 and a *feoB* mutant were then tested for their ability to invade human INT-407 embryonic intestinal cells and porcine IPEC-1 small intestinal epithelial cells. Both strains were equally able to invade both types of cells and survive for up to 48 h. However, after 48 h the *feoB* mutant exhibited a decreased ability to survive in the eukaryotic cells indicating that *feoB* contributes to intracellular survival in *C. jejuni* (Naikare et al. 2006). The *feoB* mutants examined in this study also exhibited a decreased ability to colonize in a chick cecum model and in a rabbit ileal loop model demonstrating that FeoB is important for colonization within the host (Naikare et al. 2006). Lastly, *C. jejuni* WT strains and *feoB* mutants were examined for their ability to colonize in a piglet intestine to simulate infection and colonization in a human host. Three days post-infection, different parts of the gastrointestinal tract of the piglets were harvested and through competition assays it was determined that *feoB* mutants were unable to colonize in the intestinal tract of the piglets (Naikare et al. 2006).

Francisella tularensis is responsible for zoonotic tularemia infections, is highly infectious, and has a high mortality rate, which can be linked in part to Feo utilization (Thomas-Charles et al. 2013). *F. tularensis* Δ*feoB* strains exhibit reduced colony size as a result of inefficient Fe^{2+} uptake, and this strain exhibited significantly slower growth in iron-restricted medium compared to the WT strain. The loss of FeoB also results in increased secretion of the rhizoferrin-like siderophore encoded by the *fsl* operon suggesting that *F. tularensis* attempts to overcome the loss of FeoB through an alternative iron uptake system (Thomas-Charles et al. 2013). The Δ*feoB* strain also contained significantly reduced cellular iron content, which could be restored with complementation. Unsurprisingly, the strain displayed significantly reduced replication in human lung epithelial cells and macrophages. However, despite the lack of a functional *feoB*, the deletion strain still caused 100% mortality rate in infected mice; however, at 3 days post-infection, the lungs, livers and spleens were collected to analyze the presence of each strain and it was determined that the Δ*feoB* strain was present in reduced quantities (Thomas-Charles et al. 2013). Another study of *F. tularensis* Schu4 demonstrated that FeoB was similarly necessary for bacterial growth, Fe^{2+} uptake under both iron-replete and iron-deplete conditions, and that in a Δ*feoB'* (encoding FeoB without the C-terminus) strain the *fsl* operon displayed increased expression (Pérez et al. 2016). The Δ*feoB'* strain could replicate within murine macrophages but showed reduced replication in human liver carcinoma cells. A double deletion strain also lacking the *fslA* gene could not replicate within the murine macrophages or the human liver carcinoma cells. A murine model demonstrated that the Δ*feoB'* strain could kill infected mice within 5–7 days, similar to the WT *F. tularensis* Schu4, while mice infected with the

double deletion strain lived for at least 21 days post-infection, demonstrating the importance of FeoB coupled to other iron acquisition systems for full bacterial virulence (Pérez et al. 2016).

In a similar manner, the Feo system of the *a*vian *p*athogen *E. coli* O78 (APEC) is connected to other metal uptake routes for maximum virulence (Sabri et al. 2008). In APEC, SitABCD contributes to virulence in chickens, and strains lacking this system exhibited significantly reduced colonization. However, in the presence of a functional SitABCD system, strains carrying either a Δ*feoB* or a Δ*mntH* behaved similar to WT APEC and persisted in the chicken model, suggesting Feo and MntH are less important for APEC virulence compared to SitABCD (Sabri et al. 2008). Double deletion strains were tested for their effects on APEC virulence as well. Both a Δ*sitABCD*Δ*mntH* strain and a Δ*sitABCD*Δ*feoB* strain were just as attenuated for virulence as the Δ*sitABCD* strain, confirming the previous result that *feoB* and *mntH* do not contribute to APEC virulence as much as *sitABCD* (Sabri et al. 2008). Interestingly, the Δ*sitABCD*Δ*feoB* strain was found at lower levels in the blood, lungs, and spleen of the chicken model but was present in higher levels in the liver. These results suggest that each metal transport system may be important for colonization in certain niches within the host (Sabri et al. 2008).

Shigella flexneri infections cause dysentery in humans, and this pathogen also utilizes multiple divalent metal ion uptake systems including Feo to maintain proper metal homeostasis. Akin to APEC, a *feoB* mutant strain was modestly attenuated for growth, similar to an *iucD* mutant, which is a component of the aerobactin siderophore synthesis system. Interestingly, a double mutant of *feoB* and *iucD* grew poorly, though it is not understood why (Runyen-Janecky et al. 2003). Henle cells were utilized to determine whether the mutant *S. flexneri* could form plaques. Single mutants of *sitA*, *feoB*, and *iucD* all formed plaques comparable to WT *S. flexneri*. However, the loss of any two of the three genes resulted in reduced plaque formation and size, suggesting a link between Fe^{2+} uptake and plaque formation. Lastly, a triple mutant deficient for all three genes was fully attenuated for plaque formation (Runyen-Janecky et al. 2003). These data suggest that each Fe^{2+} transport system may be important for growth, virulence, and/or survival of *S. flexneri*.

Yersinia pestis, the pathogen responsible for bubonic, septicemic, and pneumonic plagues in humans and animals, also utilizes the Feo system for virulence. *Y. pestis* is strongly adapted to scavenge iron from its environment as it encodes up to 12 putative iron transport systems, including Feo. The Yfe system, homologous to the Sit system, transports Mn^{2+} and Fe^{2+} and has been shown to be important for pathogenesis in mice (Perry et al. 2007). *Y. pestis* encodes for its own siderophore, Yersiniabactin (Fe^{3+}-utilizing), which was previously shown to be an essential virulence factor during the early stages of infection, whereas the Yfe system (Fe^{2+}-utilizing) was indispensable for late stage infection, delineating a clear role for Fe^{3+} and Fe^{2+} at different stages of infection (Perry et al. 2007). Under microaerophilic conditions, a *Y. pestis* Δ*feoB* strain was attenuated for growth by ≈50%, nearly to the same extent as a Δ*yfe* strain. The loss of both Fe^{2+} transport systems attenuated growth further. These effects were not observed in the deletion strains growing under

oxic conditions (Perry et al. 2007). Interestingly, the FeoC protein does not appear to be essential for *Y. pestis* growth, while the loss of a functional FeoA attenuated growth to the same extent as the Δ*feoB* strain. The *Y. pestis* Δ*feoB* strain and the *Y. pestis* Δ*yfe* strain were still able to replicate intracellularly in murine macrophages, whereas a strain lacking both *feoB* and *yfe* could not replicate in the murine macrophages, indicating that one system can compensate for the loss of the other during infection (Perry et al. 2007).

A 2009 study demonstrated the importance of FeoB to the virulence of *Streptococcus suis*, a pathogen that infects swine and is responsible for septicemia and meningitis. In silico analysis of *S. suis* led to the discovery of an *feoA* gene in *S. suis* predicted to encode a larger than usual 156 amino acid protein and *feoB* was identified and predicted to encode a 714 amino acid protein. No *feoC* gene was identified (Aranda et al. 2009). Using *e*lectrophoretic *m*obility *s*hift *a*ssays (EMSAs), the *S. suis* Fur protein was found to bind specifically to the *feo* operon's promoter, and derepression of *feoA* and *feoB* expression was observed in a *fur* mutant. A murine infection model was then used to establish the contribution of *feo* to virulence. In a *feoB* mutant strain, in vitro growth of the mutant was lower in iron-depleted conditions, and virulence in mice was significantly attenuated, linking *feoB* to full virulence of *S. suis* in murine models (Aranda et al. 2009).

P. aeruginosa is an opportunistic pathogen reliant on host iron that is obtained via multiple acquisition systems, and this pathogen is the dominant infectious agent of late-stage cystic fibrosis (CF) patients. *P. aeruginosa*'s reliance on host iron is evident, as transcripts of *feoA, feoB*, *bqsR/S* (a two-component Fe^{2+} sensing system), *pvdA* (the pyoverdine biosynthetic protein), *fptA* (the ferripyochelin receptor), and *hasAp* (the heme uptake protein) have all been detected at various levels in the sputum. As CF progresses and becomes more severe, O_2 permeability of lung tissue generally decreases, and the concentration of Fe^{2+} in lung sputum increases and is correlated with declining lung function (Hunter et al. 2013). One possible source of reduced iron could come from reaction with excreted reducing agents, such as phenazines, which are redox-active compounds that can reduce Fe^{3+} to Fe^{2+}. Intriguingly, the phenazines pyocyanin and phenazine-1-carboxylic acid are present in ca. 80% of sputum samples; however, phenazine levels do not appear to correlate with increased Fe^{2+} concentrations (Hunter et al. 2013), making the source of Fe^{2+} in the CF lung unclear. Nevertheless, it has been suggested that iron in CF lungs exists in mixed oxidation states at various stages of disease progression, and that the iron composition changes over time (Hunter et al. 2013), likely an important factor for biofilms. There is also evidence that FeoB is necessary for *P. aeruginosa* to utilize Fe^{3+} derived from citrate transport across the outer membrane receptor FecA (Marshall et al. 2009). Thus Feo appears to play an important role in oxic iron transport, in addition to anoxic iron transport within *P. aeruginosa*.

CF disease progression is correlated with increased biofilm formation by *P. aeruginosa*, and iron availability is an important factor for biofilm formation. A biofilm assay under hypoxic conditions demonstrated that an Fe^{3+} chelator, conalbumin, and a Fe^{2+} chelator, ferrozine, could inhibit biofilm formation by >50%. Biofilm formation could be restored by the addition of excess iron, suggesting that

iron bioavailability is important for biofilm formation in cystic fibrosis lungs (Hunter et al. 2013). Both chelators were then tested for their ability to dissolve preformed biofilms under oxic and anoxic conditions. Significant biofilm dissolution was observed when both chelators were present. Under anoxic conditions, ferrozine alone could dissolve preformed biofilms by 20%. Biofilms reformed with the addition of iron, suggesting biofilm formation is iron-mediated (Hunter et al. 2013). This interesting corollary between biofilms and iron availability could be a future direction of exploration into the progression of CF disease.

Acinetobacter baumannii has recently been listed as one of the most dangerous opportunistic pathogens by the World Health Organization, and Feo is one of the contributing factors to this organism's virulence (Álvarez-Fraga et al. 2018). 50 clinical strains of *A. baumannii* containing the Feo operon (*feoA* and *feoB*) were previously identified, and it was found that overexpression of *feoA* occurred during infection of *A. baumannii* within the lung. A clinically-relevant strain lacking the *feoA* gene was constructed and growth of this strain was tested under both iron-sufficient and iron-limited conditions. In iron-replete media, both the Δ*feoA* and WT strains showed no differences in growth; however, the generation time of the Δ*feoA* strain was significantly higher in iron-limited media compared to the WT strain, indicating that *feoA* is important for the fitness of *A. baumannii* (Álvarez-Fraga et al. 2018). In experiments assessing biofilm formation and cellular adhesion, the inactivation of *feoA* detrimentally affected both markers of *A. baumannii* virulence. When the Δ*feoA* strain was complemented with a plasmid encoding for *feoA*, both abilities were only partially restored. Cells lacking *feoA* were also more susceptible to oxidative stress as opposed to the WT strain (Álvarez-Fraga et al. 2018). A *Galleria mellonella* (moth) infection model and a murine pneumonia model have both been used to study how *feoA* affects the virulence of this pathogen. *A. baumannii* Δ*feoA* strains were unable to infect and kill *G. mellonella*. Similarly, mice that were intratracheally infected with the Δ*feoA* strain had significantly decreased mortality rates, and the occurrence of positive sterling blood cultures for mice infected with the Δ*feoA* strain increased by 75% compared to the WT, demonstrating that *feoA* is necessary for *A. baumannii* virulence (Álvarez-Fraga et al. 2018). Thus, these results suggest that FeoA could serve as a novel therapeutic target given its strong contribution to *A. baumannii* virulence.

P. gingivalis is an oral pathogen and the causative agent of gingivitis, one of the most common human infections worldwide, and its genome contains an *feoA-feoB* fusion. *P. gingivalis* has a growth requirement for iron, but it cannot synthesize heme, does not produce siderophores, and lacks ferric iron reductase activity, necessitating Fe^{2+} uptake as one of its major routes of iron acquisition (Dashper et al. 2005). At first glance, two genes annotated as *feoB* are present in the organism (*feoB1* and *feoB2*). The *feoB1* gene was demonstrated to encode a ferrous iron transporter necessary for pathogenesis (lesion formation) in murine models, while *feoB2* was demonstrated to encode a functional manganese transporter. Interestingly, in the absence of the functional ferrous iron transporter (*feoB1*), the functional manganese transporter (*feoB2*) may be upregulated to support growth and survival, but this gene product does not support infection. This is the first example of an

FeoB-like protein transporting a metal other than ferrous iron (Dashper et al. 2005), but it remains unclear whether *feoB2* is a bona fide FeoB protein. In contrast, it is clear that the *feoB1* gene encodes for a naturally-tethered FeoA-FeoB polypeptide based on sequence conservation. Beyond this information, no work at the protein level has detailed the function of this novel fusion.

B. fragilis is a commensal bacterium that can become opportunistic when and if it enters environments outside of the gut, is becoming increasingly resistant to metronidazole (the most widely used treatment for *B. fragilis* infections), and its genome also contains an *feoA-feoB* fusion (Veeranagouda et al. 2014; Rocha et al. 2019). Intriguingly, the absence of the *feoAB* gene conferred metronidazole resistance to *B. fragilis* in one study, despite exhibiting slower growth kinetics. However, the reason for increased resistance to metronidazole in *feoAB* mutants and the effect of iron on resistance remains unknown (Rocha et al. 2019). Additionally, both heme and non-heme iron are necessary for the survival of *B. fragilis* during infection (Rocha et al. 2019). *B. fragilis* cannot synthesize heme de novo, but it has an ability to remove metal from nonferrous metallated porphyrins (dechelatase activity) and to then insert ferrous iron into the apo porphyrins (ferrochelatase activity) (Rocha et al. 2019). The acquisition of ferrous iron is thus important to heme metabolism in *B. fragilis*, and a Δ*feoAB* strain was unable to grow in the presence of heme, suggesting that iron derived from heme is necessary for growth (Rocha et al. 2019). Consistent with this hypothesis, when supplemented with 100 μM $FeSO_4$ growth of the deletion strain was rescued. It is suggested that iron is removed from heme in the periplasm and transported via FeoAB to support growth, thus linking heme metabolism and Feo-mediated Fe^{2+} uptake in this organism (Rocha et al. 2019). However, like *P. gingivalis*, work at the protein level on the *B. fragilis* FeoA-FeoB fusion is unrealized.

Finally, pathogens utilizing the Feo system also infect plants, although this host-pathogen interface is not well-studied. *Xanthomonas* is a genus of Gram-negative bacteria responsible for causing approximately 400 different diseases in plants, including bacterial blight disease in rice (Pandey and Sonti 2010). *Xanthomonas oryzae* pv. *oryzae* causes disease in the xylem vessels of rice leaves, and this pathogen encodes for a tripartite FeoA, FeoB, and FeoC system. These genes are cotranscribed when iron is both replete and limiting (Pandey and Sonti 2010). In *X. oryzae*, an *feoB* mutant was defective for growth and overproduced siderophores, while the WT strain did not, suggesting that the pathogen was trying to overcome the loss of an essential iron transport system (Pandey and Sonti 2010). Rice inoculated with the *Xanthomonas feoB* mutant produced fewer lesions than those inoculated with WT, whereas bacteria deficient for siderophore production were as virulent as WT, suggesting that the Feo system is an essential component of *in planta* virulence (Pandey and Sonti 2010).

12.6 Conclusions and Outlook

From early to present-day Earth, multiple pools of ferrous iron are important for microorganisms to meet their metabolic needs. This principle is especially true in the anoxic and acidic environments that bacteria encounter within a host or in soils, aquatic environments, or waste sites, to name a few. Given the drastic changes in environments that microbes encounter, from iron-replete to iron-depleted conditions, it is absolutely essential for iron uptake and storage to be regulated in a manner that maintains intracellular iron stores at appropriate levels and fulfills the varying metabolic needs of each organism.

Several Fe^{2+} uptake systems have been identified in bacteria, though many are not specific for Fe^{2+} and have not been well-characterized either at the cellular level or at the protein level, and thus their contribution to bacterial virulence remains unknown. In contrast, cellular studies have established the role of Feo (and in particular FeoB), the dominant prokaryotic Fe^{2+} transport system, for bacterial survival and virulence. Despite this importance, several gaps in our knowledge still remain regarding the structure of full-length FeoB and how FeoB facilitates transport of Fe^{2+} across the cytoplasmic membrane. It is unclear if a periplasmic binding protein or another chelator facilitates transfer of Fe^{2+} to FeoB, potentially through the periplasmic loop, which residues in the TM region binding and translocating Fe^{2+} across the membrane, and what happens to Fe^{2+} once it reaches the cytosol. Additional questions remain regarding the GTPase/NTPase activity of the G-protein domain of NFeoB and how nucleotide hydrolysis is linked to Fe^{2+} transport. FeoA and FeoC, both small cytosolic proteins, have been subjected to numerous studies though their functions remain undetermined. Given that FeoA can be found fused to NFeoB through a linker region to the G-protein domain, it is likely that FeoA and NFeoB interact. However, the exact site of this potential interaction and the functional implications have not been elucidated. Lastly, FeoC has been shown to bind a redox active [4Fe-4S] cluster, implying that FeoC could add an additional layer of regulation to the Feo system. However, FeoC is poorly conserved and some FeoC proteins, such as from *Vibrio* species, do not contain the conserved Cys residues required for iron-sulfur cluster binding. Undoubtedly, more experiments aimed at elucidating these details and more functional models of FeoB will be necessary to gain a better understanding of this broadly distributed Fe^{2+} transport pathway.

Despite this lack in knowledge, it is clear that ferrous iron acquisition, linked in particular to the Feo system, is important for the survival of bacterial species across multiple environments, and this point is especially true of pathogenic bacteria that are becoming alarmingly problematic. Antibiotic resistance has become one of the world's greatest public health challenges. Both the challenges and breakthroughs associated with antibiotic resistance continue to change as resistant pathogens evolve. According to a 2019 report from the Centers for Disease Control and Prevention (CDC), there are 2.8 million antibiotic-resistant infections in the United States every year which results in more than 35,000 deaths (Antibiotic resistance threats in the United States 2019). In fact, in the United States it is estimated that

deaths associated with resistant infections will outpace those associated with cancer by the year 2050. As iron acquisition is linked to pathogenesis, and bacteria lacking functional ferrous iron transport systems (such as Feo) have been shown to be avirulent or unable to colonize in a host-associated environment, a greater understanding of the mechanisms underlying ferrous iron acquisition could be leveraged for the development of new therapeutics that could help to combat the growing global emergency of antibiotic resistance.

Acknowledgements This work was supported by NIH R21 DE027803 (A. T. S.), NIH R35 GM133497 (A. T. S.), and in part by NIH T32 GM066706 (A. E. S.).

References

Abeyrathna SS, Abeyrathna NS, Thai NK, Sarkar P, D'Arcy S, Meloni G (2019) IroT/MavN is a *Legionella* transmembrane Fe(II) transporter: metal selectivity and translocation kinetics revealed by *in vitro* real-time transport. Biochemistry 58(43):4337–4342. https://doi.org/10.1021/acs.biochem.9b00658

Abu Kwaik Y, Bumann D (2013) Microbial quest for food *in vivo*: 'nutritional virulence' as an emerging paradigm. Cell Microbiol 15(6):882–890. https://doi.org/10.1111/cmi.12138

Álvarez-Fraga L, Vázquez-Ucha JC, Martínez-Guitián M, Vallejo JA, Bou G, Beceiro A, Poza M (2018) Pneumonia infection in mice reveals the involvement of the feoA gene in the pathogenesis of *Acinetobacter baumannii*. Virulence 9(1):496–509. https://doi.org/10.1080/21505594.2017.1420451

Andrews SC, Robinson AK, Rodríguez-Quiñones F (2003) Bacterial iron homeostasis. FEMS Microbiol Rev 27(2-3):215–237

Antibiotic resistance threats in the United States (2019)

Aranda J, Cortés P, Garrido ME, Fittipaldi N, Llagostera M, Gottschalk M, Barbé J (2009) Contribution of the FeoB transporter to *Streptococcus suis* virulence. Int Microbiol 12(2):137–143

Ash MR, Maher MJ, Guss JM, Jormakka M (2011) The initiation of GTP hydrolysis by the G-domain of FeoB: insights from a transition-state complex structure. PLoS One 6(8):e23355. https://doi.org/10.1371/journal.pone.0023355

Askwith C, Kaplan J (1997) An oxidase-permease-based iron transport system in *Schizosaccharomyces pombe* and its expression in *Saccharomyces cerevisiae*. J Biol Chem 272(1):401–405. https://doi.org/10.1074/jbc.272.1.401

Askwith C, Eide D, Van Ho A, Bernard PS, Li L, Davis-Kaplan S, Sipe DM, Kaplan J (1994) The FET3 gene of *S. cerevisiae* encodes a multicopper oxidase required for ferrous iron uptake. Cell 76(2):403–410. https://doi.org/10.1016/0092-8674(94)90346-8

Bazylinski DA, Frankel RB, Jannasch HW (1988) Anaerobic magnetite production by a marine, magnetotactic bacterium. Nature 334(6182):518–519. https://doi.org/10.1038/334518a0

Bearden SW, Staggs TM, Perry RD (1998) An ABC transporter system of *Yersinia pestis* allows utilization of chelated iron by *Escherichia coli* SAB11. J Bacteriol 180(5):1135–1147

Bennett BD, Brutinel ED, Gralnick JA (2015) A ferrous iron exporter mediates iron resistance in *Shewanella oneidensis* MR-1. Appl Environ Microbiol 81(22):7938–7944. https://doi.org/10.1128/AEM.02835-15

Bennett BD, Redford KE, Gralnick JA (2018) MgtE homolog FicI acts as a secondary ferrous iron importer in *Shewanella oneidensis* strain MR-1. Appl Environ Microbiol 84(6). https://doi.org/10.1128/AEM.01245-17

Bhattacharyya P (1970) Active transport of manganese in isolated membranes of *Escherichia coli*. J Bacteriol 104(3):1307–1311. https://doi.org/10.1128/JB.104.3.1307-1311.1970

Blakemore R (1975) Magnetotactic bacteria. Science 190(4212):377–379. https://doi.org/10.1126/science.170679

Bos JL, Rehmann H, Wittinghofer A (2007) GEFs and GAPs: critical elements in the control of small G proteins. Cell 129(5):865–877. https://doi.org/10.1016/j.cell.2007.05.018

Bozzi AT, Bane LB, Weihofen WA, Singharoy A, Guillen ER, Ploegh HL, Schulten K, Gaudet R (2016) Crystal structure and conformational change mechanism of a bacterial Nramp-family divalent metal transporter. Structure 24(12):2102–2114. https://doi.org/10.1016/j.str.2016.09.017

Brunori M (2010) Myoglobin strikes back. Protein Sci 19(2):195–201. https://doi.org/10.1002/pro.300

Brutinel ED, Gralnick JA (2012) Shuttling happens: soluble flavin mediators of extracellular electron transfer in *Shewanella*. Appl Microbiol Biotechnol 93(1):41–48. https://doi.org/10.1007/s00253-011-3653-0

Caccavo F, Lonergan DJ, Lovley DR, Davis M, Stolz JF, McInerney MJ (1994) *Geobacter sulfurreducens* sp. nov., a hydrogen- and acetate-oxidizing dissimilatory metal-reducing microorganism. Appl Environ Microbiol 60(10):3752–3759. https://doi.org/10.1128/AEM.60.10.3752-3759.1994

Cain TJ, Smith AT (2021) Ferric iron reductases and their contribution to unicellular ferrous iron uptake. J Inorg Biochem 218:111407. https://doi.org/10.1016/j.jinorgbio.2021.111407

Calugay RJ, Miyashita H, Okamura Y, Matsunaga T (2003) Siderophore production by the magnetic bacterium Magnetospirillum magneticum AMB-1. FEMS Microbiol Lett 218(2):371–375. https://doi.org/10.1016/S0378-1097(02)01188-6

Calugay RJ, Takeyama H, Mukoyama D, Fukuda Y, Suzuki T, Kanoh K, Matsunaga T (2006) Catechol siderophore excretion by magnetotactic bacterium Magnetospirillum magneticum AMB-1. J Biosci Bioeng 101(5):445–447. https://doi.org/10.1263/jbb.101.445

Cao J, Woodhall MR, Alvarez J, Cartron ML, Andrews SC (2007) EfeUOB (YcdNOB) is a tripartite, acid-induced and CpxAR-regulated, low-pH Fe_{2+} transporter that is cryptic in Escherichia coli K-12 but functional in *E. coli* O157:H7. Mol Microbiol 65(4):857–875. https://doi.org/10.1111/j.1365-2958.2007.05802.x

Carlson HK, Clark IC, Melnyk RA, Coates JD (2012) Toward a mechanistic understanding of anaerobic nitrate-dependent iron oxidation: balancing electron uptake and detoxification. Front Microbiol 3:57. https://doi.org/10.3389/fmicb.2012.00057

Cartron ML, Maddocks S, Gillingham P, Craven CJ, Andrews SC (2006) Feo-transport of ferrous iron into bacteria. Biometals 19(2):143–157. https://doi.org/10.1007/s10534-006-0003-2

Chao Y, Fu D (2004) Thermodynamic studies of the mechanism of metal binding to the Escherichia coli zinc transporter YiiP. J Biol Chem 279(17):17173–17180. https://doi.org/10.1074/jbc.M400208200

Christenson ET, Isaac DT, Yoshida K, Lipo E, Kim JS, Ghirlando R, Isberg RR, Banerjee A (2019) The iron-regulated vacuolar. Proc Natl Acad Sci U S A 116(36):17775–17785. https://doi.org/10.1073/pnas.1902806116

Chu BC, Garcia-Herrero A, Johanson TH, Krewulak KD, Lau CK, Peacock RS, Slavinskaya Z, Vogel HJ (2010) Siderophore uptake in bacteria and the battle for iron with the host; a bird's eye view. Biometals 23(4):601–611. https://doi.org/10.1007/s10534-010-9361-x

Cornelis P (2010) Iron uptake and metabolism in pseudomonads. Appl Microbiol Biotechnol 86(6):1637–1645. https://doi.org/10.1007/s00253-010-2550-2

Coudray N, Valvo S, Hu M, Lasala R, Kim C, Vink M, Zhou M, Provasi D, Filizola M, Tao J, Fang J, Penczek PA, Ubarretxena-Belandia I, Stokes DL (2013) Inward-facing conformation of the zinc transporter YiiP revealed by cryoelectron microscopy. Proc Natl Acad Sci U S A 110(6):2140–2145. https://doi.org/10.1073/pnas.1215455110

Crack JC, Le Brun NE, Thomson AJ, Green J, Jervis AJ (2008) Reactions of nitric oxide and oxygen with the regulator of fumarate and nitrate reduction, a global transcriptional regulator,

during anaerobic growth of *Escherichia coli*. Methods Enzymol 437:191–209. https://doi.org/10.1016/S0076-6879(07)37011-0

D'Aquino JA, Ringe D (2003) Determinants of the SRC homology domain 3-like fold. J Bacteriol 185(14):4081–4086. https://doi.org/10.1128/jb.185.14.4081-4086.2003

Dashper SG, Butler CA, Lissel JP, Paolini RA, Hoffmann B, Veith PD, O'Brien-Simpson NM, Snelgrove SL, Tsiros JT, Reynolds EC (2005) A novel *Porphyromonas gingivalis* FeoB plays a role in manganese accumulation. J Biol Chem 280(30):28095–28102. https://doi.org/10.1074/jbc.M503896200

DeLong EF, Pace NR (2001) Environmental diversity of bacteria and archaea. Syst Biol 50(4): 470–478

Derry LA (2015) Causes and consequences of mid-Proterozoic anoxia. Geophys Res Lett 42(20): 8538–8546. https://doi.org/10.1002/2015GL065333

Deshpande CN, McGrath AP, Font J, Guilfoyle AP, Maher MJ, Jormakka M (2013) Structure of an atypical FeoB G-domain reveals a putative domain-swapped dimer. Acta Crystallogr Sect F Struct Biol Cryst Commun 69(4):399–404. https://doi.org/10.1107/S1744309113005939

Dong Z, Guo S, Fu H, Gao H (2017) Investigation of a spontaneous mutant reveals novel features of iron uptake in *Shewanella oneidensis*. Sci Rep 7(1):11788. https://doi.org/10.1038/s41598-017-11987-3

Dunning JC, Ma Y, Marquis RE (1998) Anaerobic killing of oral streptococci by reduced, transition metal cations. Appl Environ Microbiol 64(1):27–33. https://doi.org/10.1128/AEM.64.1.27-33.1998

Ehrnstorfer IA, Geertsma ER, Pardon E, Steyaert J, Dutzler R (2014) Crystal structure of a SLC11 (NRAMP) transporter reveals the basis for transition-metal ion transport. Nat Struct Mol Biol 21(11):990–996. https://doi.org/10.1038/nsmb.2904

Ellermann M, Arthur JC (2017) Siderophore-mediated iron acquisition and modulation of host-bacterial interactions. Free Radic Biol Med 105:68–78. https://doi.org/10.1016/j.freeradbiomed.2016.10.489

Embree M, Qiu Y, Shieu W, Nagarajan H, O'Neil R, Lovley D, Zengler K (2014) The iron stimulon and fur regulon of *Geobacter sulfurreducens* and their role in energy metabolism. Appl Environ Microbiol 80(9):2918–2927. https://doi.org/10.1128/AEM.03916-13

Emerson D, Fleming EJ, McBeth JM (2010) Iron-oxidizing bacteria: an environmental and genomic perspective. Annu Rev Microbiol 64:561–583. https://doi.org/10.1146/annurev.micro.112408.134208

Emerson D, Scott JJ, Benes J, Bowden WB (2015) Microbial iron oxidation in the Arctic tundra and its implications for biogeochemical cycling. Appl Environ Microbiol 81(23):8066–8075. https://doi.org/10.1128/AEM.02832-15

Eng ET, Jalilian AR, Spasov KA, Unger VM (2008) Characterization of a novel prokaryotic GDP dissociation inhibitor domain from the G protein coupled membrane protein FeoB. J Mol Biol 375(4):1086–1097. https://doi.org/10.1016/j.jmb.2007.11.027

Escolar L, Pérez-Martín J, de Lorenzo V (1999) Opening the iron box: transcriptional metalloregulation by the Fur protein. J Bacteriol 181(20):6223–6229

Esther J, Sukla LB, Pradhan N, Panda S (2015) Fe (III) reduction strategies of dissimilatory iron reducing bacteria. Korean J Chem Eng 32(1):1–14. https://doi.org/10.1007/s11814-014-0286-x

Fillat MF (2014) The FUR (ferric uptake regulator) superfamily: diversity and versatility of key transcriptional regulators. Arch Biochem Biophys 546:41–52. https://doi.org/10.1016/j.abb.2014.01.029

Fischbach MA, Lin H, Liu DR, Walsh CT (2006) How pathogenic bacteria evade mammalian sabotage in the battle for iron. Nat Chem Biol 2(3):132–138. https://doi.org/10.1038/nchembio771

Ganz T (2008) Iron homeostasis: fitting the puzzle pieces together. Cell Metab 7(4):288–290. https://doi.org/10.1016/j.cmet.2008.03.008

Gauger T, Konhauser K, Kappler A (2015) Protection of phototrophic iron(II)-oxidizing bacteria from UV irradiation by biogenic iron(III) minerals: implications for early Archean banded iron formation. Geology 43(12):1067–1070. https://doi.org/10.1130/G37095.1

Gauger T, Konhauser K, Kappler A (2016) Protection of nitrate-reducing Fe(II)-oxidizing bacteria from UV radiation by biogenic Fe(III) minerals. Astrobiology 16(4):301–310. https://doi.org/10.1089/ast.2015.1365

Glass J (2015) Microbes that meddle with metals: microorganisms depend on numerous metal cofactors; these requirements in turn depend on microbial species, type of metabolism, and environmental conditions. Microbe 10:197–202. https://doi.org/10.1128/microbe.10.197.1

Grass G, Wong MD, Rosen BP, Smith RL, Rensing C (2002) ZupT is a Zn(II) uptake system in *Escherichia coli*. J Bacteriol 184(3):864–866. https://doi.org/10.1128/jb.184.3.864-866.2002

Grass G, Franke S, Taudte N, Nies DH, Kucharski LM, Maguire ME, Rensing C (2005a) The metal permease ZupT from *Escherichia coli* is a transporter with a broad substrate spectrum. J Bacteriol 187(5):1604–1611. https://doi.org/10.1128/JB.187.5.1604-1611.2005

Grass G, Otto M, Fricke B, Haney CJ, Rensing C, Nies DH, Munkelt D (2005b) FieF (YiiP) from *Escherichia coli* mediates decreased cellular accumulation of iron and relieves iron stress. Arch Microbiol 183(1):9–18. https://doi.org/10.1007/s00203-004-0739-4

Grosse C, Scherer J, Koch D, Otto M, Taudte N, Grass G (2006) A new ferrous iron-uptake transporter, EfeU (YcdN), from *Escherichia coli*. Mol Microbiol 62(1):120–131. https://doi.org/10.1111/j.1365-2958.2006.05326.x

Guerinot ML (2000) The ZIP family of metal transporters. Biochim Biophys Acta 1465(1-2):190–198. https://doi.org/10.1016/s0005-2736(00)00138-3

Guilfoyle AP, Deshpande CN, Schenk G, Maher MJ, Jormakka M (2014) Exploring the correlation between the sequence composition of the nucleotide binding G5 loop of the FeoB GTPase domain (NFeoB) and intrinsic rate of GDP release. Biosci Rep 34(6):e00158. https://doi.org/10.1042/BSR20140152

Hagelueken G, Duthie FG, Florin N, Schubert E, Schiemann O (2015) Expression, purification and spin labelling of the ferrous iron transporter FeoB from *Escherichia coli* BL21 for EPR studies. Protein Expr Purif 114:30–36. https://doi.org/10.1016/j.pep.2015.05.014

Hagelueken G, Hoffmann J, Schubert E, Duthie FG, Florin N, Konrad L, Imhof D, Behrmann E, Morgner N, Schiemann O (2016) Studies on the X-ray and solution structure of FeoB from *Escherichia coli* BL21. Biophys J 110(12):2642–2650. https://doi.org/10.1016/j.bpj.2016.05.018

Hanert H (1974) In vivo kinetics of individual development of *Gallionella ferruginea* in batch microculture. Arch Microbiol 96(1):59–74. https://doi.org/10.1007/BF00590163

Hantke K (1987) Ferrous iron transport mutants in *Escherichia coli* K12. FEMS Microbiol Lett 44(1):53–57. https://doi.org/10.1111/j.1574-6968.1987.tb02241.x

Hantke K (2003) Is the bacterial ferrous iron transporter FeoB a living fossil? Trends Microbiol 11(5):192–195

Hider RC, Kong X (2013) Iron speciation in the cytosol: an overview. Dalton Trans 42(9):3220–3229. https://doi.org/10.1039/c2dt32149a

Hsueh KL, Yu LK, Chen YH, Cheng YH, Hsieh YC, Ke SC, Hung KW, Chen CJ, Huang TH (2013) FeoC from *Klebsiella pneumoniae* contains a [4Fe-4S] cluster. J Bacteriol 195(20):4726–4734. https://doi.org/10.1128/jb.00687-13

Hu Y, Ribbe MW (2015) Nitrogenase and homologs. J Biol Inorg Chem 20(2):435–445. https://doi.org/10.1007/s00775-014-1225-3

Huang W, Wilks A (2017) Extracellular heme uptake and the challenge of bacterial cell membranes. Annu Rev Biochem 86:799–823. https://doi.org/10.1146/annurev-biochem-060815-014214

Hung KW, Juan TH, Hsu YL, Huang TH (2012a) NMR structure note: the ferrous iron transport protein C (FeoC) from *Klebsiella pneumoniae*. J Biomol NMR 53(2):161–165. https://doi.org/10.1007/s10858-012-9633-6

Hung KW, Tsai JY, Juan TH, Hsu YL, Hsiao CD, Huang TH (2012b) Crystal structure of the *Klebsiella pneumoniae* NFeoB/FeoC complex and roles of FeoC in regulation of Fe^{2+} transport

by the bacterial Feo system. J Bacteriol 194(23):6518–6526. https://doi.org/10.1128/JB.01228-12

Hunter RC, Asfour F, Dingemans J, Osuna BL, Samad T, Malfroot A, Cornelis P, Newman DK (2013) Ferrous iron is a significant component of bioavailable iron in cystic fibrosis airways. mBio 4(4). https://doi.org/10.1128/mBio.00557-13

Ikeda JS, Janakiraman A, Kehres DG, Maguire ME, Slauch JM (2005) Transcriptional regulation of sitABCD of *Salmonella enterica* serovar typhimurium by MntR and Fur. J Bacteriol 187(3):912–922. https://doi.org/10.1128/JB.187.3.912-922.2005

Isaac DT, Laguna RK, Valtz N, Isberg RR (2015) MavN is a Legionella pneumophila vacuole-associated protein required for efficient iron acquisition during intracellular growth. Proc Natl Acad Sci U S A 112(37):E5208–E5217. https://doi.org/10.1073/pnas.1511389112

Janakiraman A, Slauch JM (2000) The putative iron transport system SitABCD encoded on SPI1 is required for full virulence of *Salmonella typhimurium*. Mol Microbiol 35(5):1146–1155. https://doi.org/10.1046/j.1365-2958.2000.01783.x

Jones DS, Kohl C, Grettenberger C, Larson LN, Burgos WD, Macaladya JL (2015) Geochemical niches of iron-oxidizing acidophiles in acidic coal mine drainage. Appl Environ Microbiol 81(4):1242–1250. https://doi.org/10.1128/AEM.02919-14

Kadi N, Arbache S, Song L, Oves-Costales D, Challis GL (2008) Identification of a gene cluster that directs putrebactin biosynthesis in *Shewanella* species: PubC catalyzes cyclodimerization of N-hydroxy-N-succinylputrescine. J Am Chem Soc 130(32):10458–10459. https://doi.org/10.1021/ja8027263

Kammler M, Schön C, Hantke K (1993) Characterization of the ferrous iron uptake system of *Escherichia coli*. J Bacteriol 175(19):6212–6219. https://doi.org/10.1128/jb.175.19.6212-6219.1993

Kehres DG, Zaharik ML, Finlay BB, Maguire ME (2000) The NRAMP proteins of *Salmonella typhimurium* and *Escherichia coli* are selective manganese transporters involved in the response to reactive oxygen. Mol Microbiol 36(5):1085–1100. https://doi.org/10.1046/j.1365-2958.2000.01922.x

Kehres DG, Janakiraman A, Slauch JM, Maguire ME (2002) SitABCD is the alkaline Mn^{2+} transporter of *Salmonella enterica* serovar typhimurium. J Bacteriol 184(12):3159. https://doi.org/10.1128/JB.184.12.3159-3166.2002

Kim H, Lee H, Shin D (2012) The FeoA protein is necessary for the FeoB transporter to import ferrous iron. Biochem Biophys Res Commun 423(4):733–738. https://doi.org/10.1016/j.bbrc.2012.06.027

Kim H, Lee H, Shin D (2013) The FeoC protein leads to high cellular levels of the Fe(II) transporter FeoB by preventing FtsH protease regulation of FeoB in *Salmonella enterica*. J Bacteriol 195(15):3364–3370. https://doi.org/10.1128/jb.00343-13

Kim H, Lee H, Shin D (2015) Lon-mediated proteolysis of the FeoC protein prevents *Salmonella enterica* from accumulating the Fe(II) transporter FeoB under high-oxygen conditions. J Bacteriol 197(1):92–98. https://doi.org/10.1128/jb.01826-14

Konhauser KO, Planavsky NJ, Hardisty DS, Robbins LJ, Warchola TJ, Haugaard R, Lalonde SV, Partin CA, Oonk PBH, Tsikos H, Lyons TW, Bekker A, Johnson CM (2017) Iron formations: a global record of neoarchaean to palaeoproterozoic environmental history. Earth-Sci Rev 172:140–177. https://doi.org/10.1016/j.earscirev.2017.06.012

Koster S, Kuhlbrandt W, Yildiz O (2009a) Purification, crystallization and preliminary X-ray diffraction analysis of the FeoB G domain from *Methanococcus jannaschii*. Acta Crystallogr Sect F Struct Biol Cryst Commun 65(Pt 7):684–687. https://doi.org/10.1107/s1744309109019216

Koster S, Wehner M, Herrmann C, Kuhlbrandt W, Yildiz O (2009b) Structure and function of the FeoB G-domain from *Methanococcus jannaschii*. J Mol Biol 392(2):405–419. https://doi.org/10.1016/j.jmb.2009.07.020

Krewulak KD, Vogel HJ (2008) Structural biology of bacterial iron uptake. Biochim Biophys Acta 1778(9):1781–1804. https://doi.org/10.1016/j.bbamem.2007.07.026

Lau CK, Ishida H, Liu Z, Vogel HJ (2013) Solution structure of *Escherichia coli* FeoA and its potential role in bacterial ferrous iron transport. J Bacteriol 195(1):46–55. https://doi.org/10.1128/jb.01121-12

Lau CK, Krewulak KD, Vogel HJ (2016) Bacterial ferrous iron transport: the Feo system. FEMS Microbiol Rev 40(2):273–298. https://doi.org/10.1093/femsre/fuv049

Ledyard KM, Butler A (1997) Structure of putrebactin, a new dihydroxamate siderophore produced by *Shewanella putrefaciens*. J Biol Inorg Chem 2(1):93–97. https://doi.org/10.1007/s007750050110

Létoffé S, Heuck G, Delepelaire P, Lange N, Wandersman C (2009) Bacteria capture iron from heme by keeping tetrapyrrol skeleton intact. Proc Natl Acad Sci U S A 106(28):11719–11724. https://doi.org/10.1073/pnas.0903842106

Li SS (2005) Specificity and versatility of SH3 and other proline-recognition domains: structural basis and implications for cellular signal transduction. Biochem J 390(Pt 3):641–653. https://doi.org/10.1042/bj20050411

Li ZQ, Zhang LC, Xue CJ, Zheng MT, Zhu MT, Robbins LJ, Slack JF, Planavsky NJ, Konhauser KO (2018) Earth's youngest banded iron formation implies ferruginous conditions in the early Cambrian Ocean. Sci Rep 8(1):9970. https://doi.org/10.1038/s41598-018-28187-2

Linkous RO, Sestok AE, Smith AT (2019) The crystal structure of *Klebsiella pneumoniae* FeoA reveals a site for protein-protein interactions. Proteins 87(11):897–903. https://doi.org/10.1002/prot.25755

Liu X, Du Q, Wang Z, Zhu D, Huang Y, Li N, Wei T, Xu S, Gu L (2011) Crystal structure and biochemical features of EfeB/YcdB from Escherichia coli O157: ASP235 plays divergent roles in different enzyme-catalyzed processes. J Biol Chem 286(17):14922–14931. https://doi.org/10.1074/jbc.M110.197780

Liu L, Li S, Wang S, Dong Z, Gao H (2018) Complex iron uptake by the Putrebactin-mediated and Feo systems in *Shewanella oneidensis*. Appl Environ Microbiol 84(20). https://doi.org/10.1128/AEM.01752-18

Lovley DR (1997) Microbial Fe(III) reduction in subsurface environments. FEMS Microbiol Rev 20(3-4):305–313. https://doi.org/10.1111/j.1574-6976.1997.tb00316.x

Lovley DR, Walker DJF (2019) Protein Nanowires. Front Microbiol 10:2078. https://doi.org/10.3389/fmicb.2019.02078

Makui H, Roig E, Cole ST, Helmann JD, Gros P, Cellier MF (2000) Identification of the *Escherichia coli* K-12 Nramp orthologue (MntH) as a selective divalent metal ion transporter. Mol Microbiol 35(5):1065–1078. https://doi.org/10.1046/j.1365-2958.2000.01774.x

Mann S, Sparks N, Frankel R, Bazylinski D, Jannasch H (1990) Biomineralization of ferrimagnetic greigite (Fe3S4) and iron pyrite (FeS2) in a magnetotactic bacterium. Nature 343. https://doi.org/10.1038/343258a0

Marlovits TC, Haase W, Herrmann C, Aller SG, Unger VM (2002) The membrane protein FeoB contains an intramolecular G protein essential for Fe(II) uptake in bacteria. Proc Natl Acad Sci U S A 99(25):16243–16248. https://doi.org/10.1073/pnas.242338299

Marshall B, Stintzi A, Gilmour C, Meyer JM, Poole K (2009) Citrate-mediated iron uptake in *Pseudomonas aeruginosa*: involvement of the citrate-inducible FecA receptor and the FeoB ferrous iron transporter. Microbiology 155(Pt 1):305–315. https://doi.org/10.1099/mic.0.023531-0

Matsunaga T, Sakaguchi T, Tadakoro F (1991) Magnetite formation by a magnetic bacterium capable of growing aerobically. Appl Microbiol Biotechnol 35(5):651–655. https://doi.org/10.1007/BF00169632

Naikare H, Palyada K, Panciera R, Marlow D, Stintzi A (2006) Major role for FeoB in *Campylobacter jejuni* ferrous iron acquisition, gut colonization, and intracellular survival. Infect Immun 74(10):5433–5444. https://doi.org/10.1128/iai.00052-06

Nies DH, Silver S (1995) Ion efflux systems involved in bacterial metal resistances. J Ind Microbiol 14(2):186–199. https://doi.org/10.1007/BF01569902

Ovchinnikov S, Park H, Varghese N, Huang PS, Pavlopoulos GA, Kim DE, Kamisetty H, Kyrpides NC, Baker D (2017) Protein structure determination using metagenome sequence data. Science (New York, NY) 355(6322):294–298. https://doi.org/10.1126/science.aah4043

Pandey A, Sonti RV (2010) Role of the FeoB protein and siderophore in promoting virulence of *Xanthomonas oryzae* pv. *oryzae* on rice. J Bacteriol 192(12):3187–3203. https://doi.org/10.1128/jb.01558-09

Parrow NL, Fleming RE, Minnick MF (2013) Sequestration and scavenging of iron in infection. Infect Immun 81(10):3503–3514

Patzer SI, Hantke K (2001) Dual repression by Fe^{2+}-Fur and Mn^{2+}-MntR of the *mntH* gene, encoding an NRAMP-like Mn^{2+} transporter in *Escherichia coli*. J Bacteriol 183(16):4806–4813. https://doi.org/10.1128/JB.183.16.4806-4813.2001

Paulsen IT, Saier MH (1997) A novel family of ubiquitous heavy metal ion transport proteins. J Membr Biol 156(2):99–103. https://doi.org/10.1007/s002329900192

Pérez N, Johnson R, Sen B, Ramakrishnan G (2016) Two parallel pathways for ferric and ferrous iron acquisition support growth and virulence of the intracellular pathogen *Francisella tularensis* Schu S4. MicrobiologyOpen 5(3):453–468. https://doi.org/10.1002/mbo3.342

Perry RD, Mier I Jr, Fetherston JD (2007) Roles of the Yfe and Feo transporters of *Yersinia pestis* in iron uptake and intracellular growth. Biometals 20(3-4):699–703. https://doi.org/10.1007/s10534-006-9051-x

Perry RD, Craig SK, Abney J, Bobrov AG, Kirillina O, Mier I, Truszczynska H, Fetherston JD (2012) Manganese transporters Yfe and MntH are Fur-regulated and important for the virulence of *Yersinia pestis*. Microbiology 158(Pt 3):804–815. https://doi.org/10.1099/mic.0.053710-0

Portier E, Zheng H, Sahr T, Burnside DM, Mallama C, Buchrieser C, Cianciotto NP, Héchard Y (2015) IroT/mavN, a new iron-regulated gene involved in *Legionella pneumophila* virulence against amoebae and macrophages. Environ Microbiol 17(4):1338–1350. https://doi.org/10.1111/1462-2920.12604

Rajasekaran MB, Nilapwar S, Andrews SC, Watson KA (2010) EfeO-cupredoxins: major new members of the cupredoxin superfamily with roles in bacterial iron transport. Biometals 23(1):1–17. https://doi.org/10.1007/s10534-009-9262-z

Raphael BH, Joens LA (2003) FeoB is not required for ferrous iron uptake in *Campylobacter jejuni*. Can J Microbiol 49(11):727–731. https://doi.org/10.1139/w03-086

Richard KL, Kelley BR, Johnson JG (2019) Heme uptake and utilization by gram-negative bacterial pathogens. Front Cell Infect Microbiol 9:81. https://doi.org/10.3389/fcimb.2019.00081

Richter K, Schicklberger M, Gescher J (2012) Dissimilatory reduction of extracellular electron acceptors in anaerobic respiration. Appl Environ Microbiol 78(4):913–921. https://doi.org/10.1128/AEM.06803-11

Robey M, Cianciotto NP (2002) *Legionella pneumophila* feoAB promotes ferrous iron uptake and intracellular infection. Infect Immun 70(10):5659–5669

Rocha ER, Bergonia HA, Gerdes S, Jeffrey Smith C (2019) *Bacteroides fragilis* requires the ferrous-iron transporter FeoAB and the CobN-like proteins BtuS1 and BtuS2 for assimilation of iron released from heme. MicrobiologyOpen 8(4):e00669. https://doi.org/10.1002/mbo3.669

Roden EE, Sobolev D, Glazer B, Luther GW (2004) Potential for microscale bacterial Fe redox cycling at the aerobic-anaerobic interface. Geomicrobiol J 21(6):379–391. https://doi.org/10.1080/01490450490485872

Rong C, Huang Y, Zhang W, Jiang W, Li Y, Li J (2008) Ferrous iron transport protein B gene (feoB1) plays an accessory role in magnetosome formation in *Magnetospirillum gryphiswaldense* strain MSR-1. Res Microbiol 159(7):530–536. https://doi.org/10.1016/j.resmic.2008.06.005

Rong C, Zhang C, Zhang Y, Qi L, Yang J, Guan G, Li Y, Li J (2012) FeoB2 functions in magnetosome formation and oxidative stress protection in *Magnetospirillum gryphiswaldense* strain MSR-1. J Bacteriol 194(15):3972–3976. https://doi.org/10.1128/JB.00382-12

Runyen-Janecky LJ, Reeves SA, Gonzales EG, Payne SM (2003) Contribution of the *Shigella flexneri* Sit, Iuc, and Feo iron acquisition systems to iron acquisition in vitro and in cultured cells. Infect Immun 71(4):1919–1928

Sabri M, Caza M, Proulx J, Lymberopoulos MH, Brée A, Moulin-Schouleur M, Curtiss R 3rd, Dozois CM (2008) Contribution of the SitABCD, MntH, and FeoB metal transporters to the virulence of avian pathogenic *Escherichia coli* O78 strain chi7122. Infect Immun 76(2): 601–611. https://doi.org/10.1128/iai.00789-07

Saier MH, Tran CV, Barabote RD (2006) TCDB: the transporter classification database for membrane transport protein analyses and information. Nucleic Acids Res 34(Database issue): D181–D186. https://doi.org/10.1093/nar/gkj001

Saier MH, Reddy VS, Moreno-Hagelsieb G, Hendargo KJ, Zhang Y, Iddamsetty V, Lam KJK, Tian N, Russum S, Wang J, Medrano-Soto A (2021) The transporter classification database (TCDB): 2021 update. Nucleic Acids Res 49(D1):D461–D467. https://doi.org/10.1093/nar/gkaa1004

Schad M, Konhauser KO, Sánchez-Baracaldo P, Kappler A, Bryce C (2019) How did the evolution of oxygenic photosynthesis influence the temporal and spatial development of the microbial iron cycle on ancient earth? Free Radic Biol Med 140:154–166. https://doi.org/10.1016/j.freeradbiomed.2019.07.014

Schröder I, Johnson E, de Vries S (2003) Microbial ferric iron reductases. FEMS Microbiol Rev 27(2-3):427–447. https://doi.org/10.1016/S0168-6445(03)00043-3

Schüler D, Baeuerlein E (1998) Dynamics of iron uptake and Fe3O4 biomineralization during aerobic and microaerobic growth of *Magnetospirillum gryphiswaldense*. J Bacteriol 180(1): 159–162

Seeliger S, Cord-Ruwisch R, Schink B (1998) A periplasmic and extracellular c-type cytochrome of *Geobacter sulfurreducens* acts as a ferric iron reductase and as an electron carrier to other acceptors or to partner bacteria. J Bacteriol 180(14):3686–3691. https://doi.org/10.1128/JB.180.14.3686-3691.1998

Sestok AE, Linkous RO, Smith AT (2018) Toward a mechanistic understanding of Feo-mediated ferrous iron uptake. Metallomics 10(7):887–898. https://doi.org/10.1039/c8mt00097b

Sestok AE, Lee MA, Smith AT (2021) Unpublished results

Severance S, Chakraborty S, Kosman DJ (2004) The Ftr1p iron permease in the yeast plasma membrane: orientation, topology and structure-function relationships. Biochem J 380(Pt 2): 487–496. https://doi.org/10.1042/BJ20031921

Seyedmohammad S, Born D, Venter H (2014) Expression, purification and functional reconstitution of FeoB, the ferrous iron transporter from *Pseudomonas aeruginosa*. Protein Expr Purif 101:138–145. https://doi.org/10.1016/j.pep.2014.06.012

Seyedmohammad S, Fuentealba NA, Marriott RA, Goetze TA, Edwardson JM, Barrera NP, Venter H (2016) Structural model of FeoB, the iron transporter from *Pseudomonas aeruginosa*, predicts a cysteine lined, GTP-gated pore. Biosci Rep 36(2). https://doi.org/10.1042/bsr20160046

Sheldon JR, Heinrichs DE (2015) Recent developments in understanding the iron acquisition strategies of gram positive pathogens. FEMS Microbiol Rev 39(4):592–630. https://doi.org/10.1093/femsre/fuv009

Shih PM (2019) Early cyanobacteria and the innovation of microbial sunscreens. mBio 10(3). https://doi.org/10.1128/mBio.01262-19

Shin M, Mey AR, Payne SM (2019) FeoB contains a dual nucleotide-specific NTPase domain essential for ferrous iron uptake. Proc Natl Acad Sci U S A 116(10):4599–4604. https://doi.org/10.1073/pnas.1817964116

Shin M, Park J, Jin Y, Kim IJ, Payne SM, Kim KH (2020) Biochemical characterization of bacterial FeoBs: a perspective on nucleotide specificity. Arch Biochem Biophys 685:108350. https://doi.org/10.1016/j.abb.2020.108350

Silver S, Kralovic ML (1969) Manganese accumulation by *Escherichia coli*: evidence for a specific transport system. Biochem Biophys Res Commun 34(5):640–645. https://doi.org/10.1016/0006-291x(69)90786-4

Silver S, Johnseine P, King K (1970) Manganese active transport in *Escherichia coli*. J Bacteriol 104(3):1299–1306. https://doi.org/10.1128/JB.104.3.1299-1306.1970

Simmons SL, Sievert SM, Frankel RB, Bazylinski DA, Edwards KJ (2004) Spatiotemporal distribution of marine magnetotactic bacteria in a seasonally stratified coastal salt pond. Appl Environ Microbiol 70(10):6230–6239. https://doi.org/10.1128/AEM.70.10.6230-6239.2004

Skaar EP (2010) The battle for iron between bacterial pathogens and their vertebrate hosts. PLoS Pathog 6(8):e1000949. https://doi.org/10.1371/journal.ppat.1000949

Smith AT, Sestok AE (2018) Expression and purification of functionally active ferrous iron transporter FeoB from *Klebsiella pneumoniae*. Protein Expr Purif 142:1–7. https://doi.org/10.1016/j.pep.2017.09.007

Smith RL, Thompson LJ, Maguire ME (1995) Cloning and characterization of MgtE, a putative new class of Mg^{2+} transporter from *Bacillus firmus* OF4. J Bacteriol 177(5):1233–1238. https://doi.org/10.1128/jb.177.5.1233-1238.1995

Smith JA, Lovley DR, Tremblay PL (2013) Outer cell surface components essential for Fe(III) oxide reduction by *Geobacter metallireducens*. Appl Environ Microbiol 79(3):901–907. https://doi.org/10.1128/AEM.02954-12

Smith AT, Linkous RO, Max NJ, Sestok AE, Szalai VA, Chacón KN (2019) The FeoC [4Fe-4S] cluster is redox-active and rapidly oxygen-sensitive. Biochemistry 58(49):4935–4949. https://doi.org/10.1021/acs.biochem.9b00745

Soe CZ, Codd R (2014) Unsaturated macrocyclic dihydroxamic acid siderophores produced by *Shewanella putrefaciens* using precursor-directed biosynthesis. ACS Chem Biol 9(4):945–956. https://doi.org/10.1021/cb400901j

Spiro S, Guest JR (1990) FNR and its role in oxygen-regulated gene expression in *Escherichia coli*. FEMS Microbiol Rev 6(4):399–428

Stearman R, Yuan DS, Yamaguchi-Iwai Y, Klausner RD, Dancis A (1996) A permease-oxidase complex involved in high-affinity iron uptake in yeast. Science 271(5255):1552–1557. https://doi.org/10.1126/science.271.5255.1552

Stevenson B, Wyckoff EE, Payne SM (2016) *Vibrio cholerae* FeoA, FeoB, and FeoC interact to form a complex. J Bacteriol 198(7):1160–1170. https://doi.org/10.1128/jb.00930-15

Sturm A, Schierhorn A, Lindenstrauss U, Lilie H, Brüser T (2006) YcdB from Escherichia coli reveals a novel class of Tat-dependently translocated hemoproteins. J Biol Chem 281(20):13972–13978. https://doi.org/10.1074/jbc.M511891200

Su YC, Chin KH, Hung HC, Shen GH, Wang AH, Chou SH (2010) Structure of Stenotrophomonas maltophilia FeoA complexed with zinc: a unique prokaryotic SH3-domain protein that possibly acts as a bacterial ferrous iron-transport activating factor. Acta Crystallogr Sect F Struct Biol Cryst Commun 66(Pt 6):636–642. https://doi.org/10.1107/s1744309110013941

Suzuki T, Okamura Y, Calugay RJ, Takeyama H, Matsunaga T (2006) Global gene expression analysis of iron-inducible genes in *Magnetospirillum magneticum* AMB-1. J Bacteriol 188(6):2275–2279. https://doi.org/10.1128/JB.188.6.2275-2279.2006

Suzuki T, Okamura Y, Arakaki A, Takeyama H, Matsunaga T (2007) Cytoplasmic ATPase involved in ferrous ion uptake from magnetotactic bacterium M*agnetospirillum magneticum* AMB-1. FEBS Lett 581(18):3443–3448. https://doi.org/10.1016/j.febslet.2007.06.047

Taoka A, Umeyama C, Fukumori Y (2009) Identification of iron transporters expressed in the magnetotactic bacterium *Magnetospirillum magnetotacticum*. Curr Microbiol 58(2):177–181. https://doi.org/10.1007/s00284-008-9305-7

Thomas-Charles CA, Zheng H, Palmer LE, Mena P, Thanassi DG, Furie MB (2013) FeoB-mediated uptake of iron by *Francisella tularensis*. Infect Immun 81(8):2828–2837. https://doi.org/10.1128/iai.00170-13

Thormann KM, Saville RM, Shukla S, Pelletier DA, Spormann AM (2004) Initial phases of biofilm formation in *Shewanella oneidensis* MR-1. J Bacteriol 186(23):8096–8104. https://doi.org/10.1128/JB.186.23.8096-8104.2004

Torrents E (2014) Ribonucleotide reductases: essential enzymes for bacterial life. Front Cell Infect Microbiol 4:52. https://doi.org/10.3389/fcimb.2014.00052

Troxell B, Hassan HM (2013) Transcriptional regulation by ferric uptake regulator (Fur) in pathogenic bacteria. Front Cell Infect Microbiol 3:59. https://doi.org/10.3389/fcimb.2013.00059

Unden G, Achebach S, Holighaus G, Tran HG, Wackwitz B, Zeuner Y (2002) Control of FNR function of Escherichia coli by O2 and reducing conditions. J Mol Microbiol Biotechnol 4(3): 263–268

Veeranagouda Y, Husain F, Boente R, Moore J, Smith CJ, Rocha ER, Patrick S, Wexler HM (2014) Deficiency of the ferrous iron transporter FeoAB is linked with metronidazole resistance in *Bacteroides fragilis*. J Antimicrob Chemother 69(10):2634–2643. https://doi.org/10.1093/jac/dku219

Velayudhan J, Hughes NJ, McColm AA, Bagshaw J, Clayton CL, Andrews SC, Kelly DJ (2000) Iron acquisition and virulence in *Helicobacter pylori*: a major role for FeoB, a high-affinity ferrous iron transporter. Mol Microbiol 37(2):274–286

Vetter IR, Wittinghofer A (2001) The guanine nucleotide-binding switch in three dimensions. Science 294(5545):1299–1304. https://doi.org/10.1126/science.1062023

Weaver EA, Wyckoff EE, Mey AR, Morrison R, Payne SM (2013) FeoA and FeoC are essential components of the *Vibrio cholerae* ferrous iron uptake system, and FeoC interacts with FeoB. J Bacteriol 195(21):4826–4835. https://doi.org/10.1128/jb.00738-13

Weber KA, Achenbach LA, Coates JD (2006) Microorganisms pumping iron: anaerobic microbial iron oxidation and reduction. Nat Rev Microbiol 4(10):752–764. https://doi.org/10.1038/nrmicro1490

Wei Y, Fu D (2005) Selective metal binding to a membrane-embedded aspartate in the Escherichia coli metal transporter YiiP (FieF). J Biol Chem 280(40):33716–33724. https://doi.org/10.1074/jbc.M506107200

Winterbourn CC (1995) Toxicity of iron and hydrogen peroxide: the Fenton reaction. Toxicol Lett 82-83:969–974

Wittenberg JB, Bolognesi M, Wittenberg BA, Guertin M (2002) Truncated hemoglobins: a new family of hemoglobins widely distributed in bacteria, unicellular eukaryotes, and plants. J Biol Chem 277(2):871–874. https://doi.org/10.1074/jbc.R100058200

Xia M, Wei J, Lei Y, Ying L (2007) A novel ferric reductase purified from *Magnetospirillum gryphiswaldense* MSR-1. Curr Microbiol 55(1):71–75. https://doi.org/10.1007/s00284-007-0023-3

Zhang C, Meng X, Li N, Wang W, Sun Y, Jiang W, Guan G, Li Y (2013) Two bifunctional enzymes with ferric reduction ability play complementary roles during magnetosome synthesis in *Magnetospirillum gryphiswaldense* MSR-1. J Bacteriol 195(4):876–885. https://doi.org/10.1128/JB.01750-12

Zhou D, Hardt WD, Galán JE (1999) *Salmonella typhimurium* encodes a putative iron transport system within the centisome 63 pathogenicity island. Infect Immun 67(4):1974–1981